KAUNAS UNIVERSITY OF TECHNOLOGY
LITHUANIAN ENERGY INSTITUTE

PAULIUS VILKINIS

INVESTIGATION OF FLOW DYNAMICS AND STRUCTURE IN CHANNELS WITH STRUCTURED SURFACES

Summary of Doctoral Dissertation

Technological Sciences, Energetics and Power Engineering (T 006)

2019, Kaunas

Dissertation was prepared during the period 2015-2019 at Lithuanian Energy Institute, Laboratory of heat equipment research and testing. The studies were supported by Research Council of Lithuania.

Scientific Supervisor:

Dr. Nerijus PEDIŠIUS (Lithuanian Energy Institute, Technological Sciences, Energetic and Power Engineering – T 006).

Editor: Jūratė Kulčickytė-Gutaitė

Dissertation Defence Board of Energetics and Power Engineering Science Field:

Prof. Dr. Habil. Gintautas MILIAUSKAS (Kaunas University of Technology, Technological Sciences, Energetics and Power Engineering – T 006) – **Chairman,**

Dr. Algis DŽIUGYS (Lithuanian Energy Institute, Technological Sciences, Energetics and Power Engineering – T 006),

Prof. Dr. Algirdas JASINSKAS (Vytautas Magnus University Agriculture Academy, Technological Sciences, Environmental Engineering – T 004),

Dr. Raimondas PABARČIUS (Lithuanian Energy Institute, Technological Sciences, Energetics and Power Engineering – T 006),

Prof. Dr. Jacek POZORSKI (Polish Academy of Science, Technological Sciences, Energetics and Power Engineering – T 006).

The official defence of the dissertation will be held at 1 p.m. on 24 January, 2020 at the public meeting of Dissertation Defence Board of Energetics and Power Engineering Science Field in Meeting Hall at Lithuanian Energy Institute.

Address: Breslaujos str. 3-202, 44403 Kaunas, Lithuania.
Tel. no (+370) 37 300 042; fax. (+370) 37 324 144; e-mail doktorantura@ktu.lt

Summary of doctoral dissertation was sent on 20th December, 2019.
The doctoral dissertation is available on the internet http://ktu.edu and at the libraries of Kaunas University of Technology (K. Donelaičio str. 20, 44239 Kaunas, Lithuania) and Lithuanian Energy Institute (Breslaujos str. 3, 44403 Kaunas, Lithuania)

KAUNO TECHNOLOGIJOS UNIVERSITETAS
LIETUVOS ENERGETIKOS INSTITUTAS

PAULIUS VILKINIS

SKYSČIO SRAUTO DINAMIKOS IR STRUKTŪROS TYRIMAS KANALUOSE SU STRUKTŪRIZUOTAIS PAVIRŠIAIS

Daktaro disertacijos santrauka

Technologijos mokslai, energetika ir termoinžinerija (T 006)

2019, Kaunas

Disertacija rengta 2015-2019 metais Lietuvos energetikos institute, Šiluminių įrengimų tyrimo ir bandymo laboratorijoje. Mokslinius tyrimus rėmė Lietuvos mokslo taryba.

Mokslinis vadovas:

Dr. Nerijus PEDIŠIUS (Lietuvos energetikos institutas, technologijos mokslai, energetika ir termoinžinerija – T 006).

Redagavo: Jūratė Kulčickytė-Gutaitė

Energetikos ir termoinžinerijos mokslo krypties disertacijos gynimo taryba:

Prof. Habil. Dr. Gintautas MILIAUSKAS (Kauno technologijos universitetas, technologijos mokslai, energetika ir termoinžinerija – T 006) (pirmininkas),

Dr. Algis DŽIUGYS (Lietuvos energetikos institutas, technologijos mokslai, energetika ir termoinžinerija – T 006),

Prof. Dr. Algirdas JASINSKAS (Vytauto Didžiojo Universiteto Žemės ūkio akademija, technologiniai mokslai, aplinkos inžinerija – T 004),

Dr. Raimondas PABARČIUS (Lietuvos energetikos institutas, technologijos mokslai, energetika ir termoinžinerija – T 006),

Prof. Dr. Jacek POZORSKI (Lenkijos mokslų akademija, technologiniai mokslai, energetika ir termoinžinerija – T 006).

Disertacija bus ginama viešame energetikos ir termoinžinerijos mokslo krypties disertacijos gynimo tarybos posėdyje 2020 m. sausio mėn. 24 d. 13 val. Lietuvos energetikos instituto posėdžių salėje.

Adresas: Breslaujos g. 3-202, 44403 Kaunas, Lietuva.
Tel. (+370) 37 300 042; faks. (+370) 37 324 144; el. paštas doktorantura@ktu.lt.

Disertacijos santrauka išsiųsta 2019 m. gruodžio 20 d.
Su disertacija galima susipažinti internetinėje svetainėje http://ktu.edu, Kauno technologijos universiteto bibliotekoje (K. Donelaičio g. 20, 44239 Kaunas) ir Lietuvos energetikos instituto skaitykloje (Breslaujos g. 3, 44403 Kaunas).

THE CONTENT OF THE SUMMARY OF DOCTORAL DISSERTATION

INTRODUCTION

Relevance of the research

Flow separation phenomena have a considerable impact on mass, momentum, and heat transfer processes in flowing fluids and their mixing processes. These phenomena are the main reason why separated flow remains a research object in engineering. Furthermore, they are a source for a deeper understanding of the internal mechanism of vortex formation, interaction, and disintegration, as well as a factor for the improvement of numerical simulation methods. Effects caused by flow separation and recirculation, in various geometries, are commonly encountered in many engineering problems (D'Adamo, Sosa, & Artana, 2014; Haddadi & Di Carlo, 2017; Kherbeet, Mohammed, Munisamy, & Salman, 2014; Pouryoussefi, Mirzaei, & Hajipour, 2015) and in various processes in biomedical (Jang et al., 2011; Jung, Kuo, Peles, & Amitay, 2012) and environmental applications (Toja-Silva, Peralta, Lopez-Garcia, Navarro, & Cruz, 2015).

The application of new experimental research techniques extends the possibilities of deeper understanding of flow structure. Analysis of complicated flow structure revealing shapes of vortices, growing cycles and other parameters become possible due to the rapid improvement of flow visualization techniques, such as micro-particle image velocimetry (μPIV) which application in flow visualization research is still increasing (Basu, Zahoor, & Khan, 2019; Xia et al., 2017; Zhai, Xia, Chen, & Li, 2016). Flow visualization techniques allow performing experimental measurements of flow parameters in undisturbed flow. Also, a combination of experimental techniques with computational fluid dynamics approach complements each other with quantitative and qualitative analyses.

Processes that are taking place in small scale channels are getting more and more attention regarding the increasing number of devices where flow in such channels is an essential part of their operation. Due to high surface-to-volume ratio, small scale channels receive more attention in designing cooling mechanisms in electronic devices (Basu et al., 2019; Rai et al., 2018; Xia et al., 2017). Development and increasing number of applications of lab-on-chip and microelectromechanical systems lead to the development of research of mixing processes in small scale channels (Chen, Li, Zeng, Hu, & Fu, 2016; Su, Chen, & Kenig, 2015; Ward & Fan, 2015). Regarding the usage of small fluid volume, knowledge of flow structure and dynamics in small scale channels is demanding in the development of various biomedical engineering devices. For instance, concerning the formation of separated shear layer and recirculating flows, cavities in small scale channels are employed in cell docking (Jang et al., 2011; Khabiry et al., 2009), trapping (Karimi, Yazdi, & Ardekani, 2013; Nilsson, Evander, Hammarström, & Laurell, 2009; Zhou, Kasper, & Papautsky, 2013)

and separation devices (Guan et al., 2013). Also, small scale channels are convenient for analysis of blood flow (Anastasiou, Spyrogianni, & Paras, 2010; Kim, Antaki, & Massoudi, 2016; Lima, Wada, Takeda, Tsubota, & Yamaguchi, 2007; Lima et al., 2008; Omori, Imai, Kikuchi, Ishikawa, & Yamaguchi, 2015), formation of blood clot as well as investigation of blood flow in aneurysms (Carlsohn, Kemmling, Petersen, & Wietzke, 2016; Lieber, Livescu, Hopkins, & Wakhloo, 2002).

Object of the research

Hydrodynamic mass transfer processes in the cavities.

The aim of the Doctoral Dissertation

The aim of this work is to investigate fluid flow dynamics and structure in channels with abrupt cross-section changes and to determine the characteristics of recirculating flow depending on flow regime and channel geometrical parameters using experimental and numerical approaches.

Tasks of the Doctoral Dissertation

In order to achieve the objective, the following tasks should be solved:

1. To determine the patterns of recirculation zone length dynamics in transitional and closed-type cavities in laminar flow regime.
2. To determine the influence of flow regime to dynamics and structure of recirculating zone in the transitional-type cavity.
3. To determine the patterns of recirculation zone length dynamics in transitional and closed-type cavities in turbulent flow regime.
4. To determine the influence of channel expansion ratio to recirculation zone length dynamics in transitional and closed-type cavities.
5. To determine the influence of flow regime to the structure of recirculating flow in deep open-type cavity.

Scientific novelty

Improved the knowledge of recirculation zone structure and length dynamics for different cavity types, depending on cavity geometrical parameters (H/h and L/h_1). Also, determined dependencies and patterns of physical recirculation zone parameters for laminar and turbulent flow regimes. Revealed causes of the effect of channel expansion ratio (H/h) and Re for dynamics of recirculation zone length, which helps to explain the scattering of other authors' results and suggest possible scaling for laminar and turbulent flow regimes.

It is shown that in the deep open-type cavity in the case of a turbulent flow regime occurs bifurcation of the primary vortex into two symmetrical structures determined by transverse flows.

Practical value

Results of this work are significant for a large number of engineering problems where flow separation is induced by abrupt changes of channel cross-section, which can be analyzed as flows over cavities in a channel. These results are useful for designing flow meters, heat sinks and mixing devices, as well as improving CFD models.

Found dependencies allow us to evaluate the location where the separated shear layer reattaches to the bottom wall of the cavity. Recirculation zone length provides information about the increased mixing zone in the cavity, also, the location of shear layer reattachment is characterized by increased heat transfer.

Statements carried out for defence

1. In transitional and closed-type cavities recirculation zone is stable and its length depends on Re_{h1} and channel expansion ratio (H/h) in the laminar flow regime.
2. When the channel expansion ratio (H/h) reaches its critical value, recirculation zone length gradually increases with Re_{h1} approaching asymptotical values characteristic to a turbulent flow regime.
3. In transitional and closed-type cavities in the case of turbulent flow regime periodical vortex formation and the growing cycle takes place, therefore, recirculation zone length does not longer depend on cavity geometrical parameters while increasing Re_{h1}.
4. In a deep open-type cavity in the case of a turbulent flow regime complex tree-dimensional flow structure is formed, characterized by vortex bifurcation and transverse flows.
5. High-frequency pulsatile flow stabilizes velocity distribution in the deep open-type cavity.

The structure and content of the Doctoral Dissertation

The dissertation is structured as follows: introduction, literature review, methodology, results, and discussion, conclusions, the list of references and the list of scientific publications. The dissertation consists of 110 pages, including 59 figures, 3 tables, and 137 references.

Scientific approbation of dissertation

Research results presented in the dissertation were published in 2 scientific articles in publication with a citation index at the “Clarivate Analytics” database “Web of Science Core Collection” and 2 scientific articles in other scientific journals. Research results were also presented at 6 international conferences.

1. LITERATURE REVIEW

1.1. Cavities types and classification

Three major flow types occur in the cavity depending on geometrical parameters. The type of cavity is determined by the ratio between the length of the cavity *L* and its depth h_1 as shown in Fig. 1. Open-type cavity is when $L/h_1 <$ 6–8. This type can also be described as a *deep* cavity. Closed-type cavity flow is when $L/h_1 >$ 12–14. Respectively, this type of cavity can be described as a *shallow*. In this type of cavity flow reattachment to the bottom of the cavity is observed. In the case of large L/h_1 values, when the influence of the forward-facing step is negligible, flow in the closed-type cavity becomes similar to flow over a widely investigated backward-facing step. The transitional-type cavity has L/h_1 values that fall between open and closed-types. This type of cavity can be characterized by flow fields observed in both open and closed-types cavities depending on the flow regime.

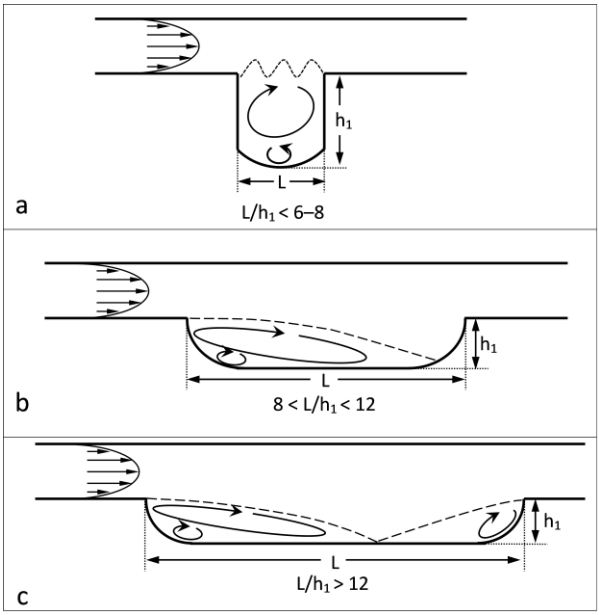

Fig. 1. Classification of cavities according to the length-to-depth ratio (L/h_1) and schematic flow structure in each type of cavity, a) open-type, b) transitional-type and c) closed-type cavity

1.2. Review of flow over cavities and obstacles

Flow separation, caused by an abrupt single expansion of the channel cross-section, is the most frequently investigated phenomenon in previous and recent scientific studies. It has been unassailably demonstrated that flow dynamics is governed by the development of a mixing layer between the main and recirculation flow, formed behind the step or obstacles and elongated to the mixing layer reattaching to the wall. The reattachment length in laminar flow increases almost linearly with an increasing Reynolds number, as observed in Fig. 2. However, the rate of reattachment length growth strongly varies depending on the shape of the cavity or obstacle. The transition to turbulent flow is another factor that determines the drastic dispersion of reattachment length values. In fully developed turbulent flow, relative values of the reattachment length are less dependent on the factors mentioned above. This means that the reattachment length, in such a flow regime, becomes directly proportional to the height of the abrupt step in a channel cross-section.

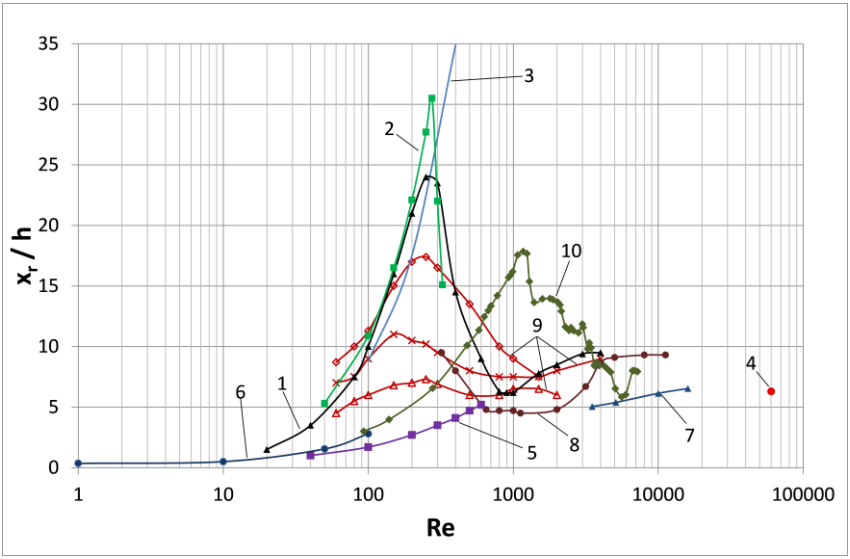

Fig. 2. Dependence of the recirculation zone length on Re from various studies in different geometries: axisymmetric expansion (curves 1–3), backward-facing step (curves 4–7 and 10), obstacles (curves 8–9). 1 – (Back & Roschke, 1972), 2 – (Gong, Liu, Chou, & Chiang, 1996), 3 – (Cantwell, Barkley, & Blackburn, 2010), 4 – (Fernando, Kriegseis, & Rival, 2012), 5 – (Goharzadeh & Rodgers, 2009), 6 – (Jayaraj, Saleel, & Shaija, 2013), 7 – (Spazzini, Iuso, Onorato, Zurlo, & Di Cicca, 2001), 8 – (Pedišius & Šlančiauskas, 1995), 9 – (Carvalho, Durst, & Pereira, 1987), 10 – (Armaly, Durst, Pereira, & Schönung, 1983). Note: Re is determined according to characteristic geometric parameters used by the authors

Arguably, the reason for changes in such consistent separated flow patterns lies within the drastic developments of the inner flow structure with a changing flow regime. Essential aspects of the cyclic growth and successive breakdown of vortices, behind the backward-facing step in flat channels and turbulent flow, using a flow visualization technique, have been analyzed and presented by Spazzini et al. (2001). According to the authors, the secondary vortex grows in strength and size until its dimensions become of comparable size to the step height and then breaks down. Wee, Yi, Annaswamy, & Ghoniem (2004) observed small vortices being generated at a short distance downstream of the backward-facing step. The vortices merge with the primary vortex, which is spread near the averaged location of the reattachment point. Henderson, Badcock, & Richards (2000) investigated a time-dependent flow structure in a transitional-type cavity at a subsonic flow velocity. During the cycle, dumbbell-like flow structure changes appear in the vortex system, which consists of an elongated primary vortex near the leading edge and a weakened small vortex near the trailing edge, which, at the end of the cycle, is absorbed by the primary vortex. A time-averaged flow pattern consists of a single elongated vortex at the leading edge, occupying most of the cavity, with reattachment to the bottom wall of the cavity. Coleman, Nikora, McLean, & Schlicke (2007) and Leonardi et al. (2003) investigated turbulent flow in rectangular cavities, separated by square bars. In the case of a transitional-type cavity, flow is comprised of two opposite-rotating vortices, where a large recirculation region is located upstream and a small one near the forward-facing step.

The three-dimensional structure of flow in the open-type cavity has been widely investigated over the past decades. Migeon, Pineau, & Texier (2003) showed that quasi-toroidal corner vortices develop near side walls in square and rectangular cross-section open-type cavities at Re = 1000. These vortices have a centrifugal origin and surround the primary eddy core. Coutanceau, Migeon, & Ehrmann (2000) showed that Taylor-Gortler-like vortices and corner vortices formats in the cylindrical semi-circular shell. These vortical structures become blurred after a short period as Reynolds number increases because of the onset of turbulence. These authors also proposed a vortical schematic structure in semi-circular geometry. Faure, Pastur, Lusseyran, Fraigneau, & Bisch (2009) investigated vortex morphology in open-type cavities with a different cavity aspect ratio and span ratio. The authors found that centrifugal instabilities are generated in open-type cavity flow. The amount of instabilities highly depends on cavity geometry. The amount of Görtler-like type vortices on the floor of the cavity increases as the cavity aspect ratio decreases and span ratio increases. The Görtler-like type vortices are developing in a spanwise row, but structures disappear at a small span ratio. Yao, Cooper, & Raghunathan (2005) numerically showed that the appearance and structure of longitudinal vortices in an open-type cavity depend on Re number and boundary layers thickness. Feldman (2015)

found that in diagonally lid-driven cavity existence of oscillation amplitude peak is the result of centrifugal effects of the flow.

As can be seen from the literature review, recirculation zone dynamics and structure is mostly analysed in the case of flow over the backward-facing step. Also, there is a lack of summarising research of dependence of recirculation zone dynamics patterns on cavity geometrical parameters which could reveal physical causes of changes in recirculation zone structure.

In summary of the literature review, essential elements influencing the dynamics and structure of recirculating flow can be identified. In view of the experience of other scientists and the results obtained, the decision was made to carry out the following experiments:

- To measure recirculating zone length in transitional and closed-type cavities depending on flow regime in the range of $1 \leq Re_{Dh} \leq 2000$ using experimental and $1 \leq Re_{Dh} \leq 10^5$ – using numerical approaches.
- To determine the dependence of relative recirculation zone length on the relative length of the cavity in the range of $4 \leq L/h_1 \leq 32$.
- To determine the influence of channel expansion ratio (H/h) to recirculation zone dynamics in transitional and closed-type cavities.
- To compare relative recirculation zone length patterns depending on Re number based on channel hydraulic diameter and depth of the cavity.
- To investigate flow structure in a deep open-type cavity depending on the flow regime in the channel.

2. METHODOLOGY

2.1. Micro-particle image velocimetry

Flow velocity vector fields and velocity profiles were obtained by a micro-particle image velocimetry system (μPIV). μPIV is an optical method used to measure fluid motion in small diameter channels. The principal scheme of the μPIV system is presented in Fig. 3. A laser sheet illuminates fluorescent tracer particles. Excited particles generate fluorescence signal, which is collected by CCD camera.

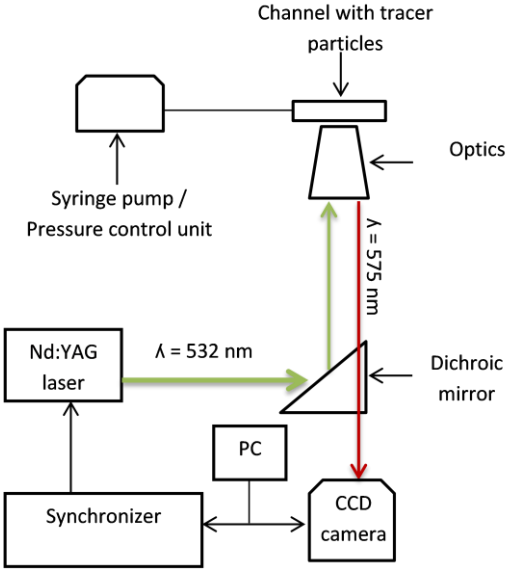

Fig. 3. Principal scheme of μPIV system

The final measurement result, the mean velocity vector field, was obtained by capturing image pairs of the tracer particles at a 15 Hz frequency. The time interval within the image frames varied from 5×10^{-3} s to 1×10^{-5} s, depending on the flow rate. In this way, time-averaged velocity data were obtained by averaging flow images during 13.3 s of flow.

The μPIV system provided by Dantec Dynamics consists of double pulsed neodymium-doped yttrium aluminum garnet (Nd: YAG) laser, laser control system LPU 450, FlowSense EO CCD camera providing an image field of 2048x2048 pixels mounted on the inverted Leica DM ILM microscope. Objective lenses of 20x magnification and 0.4 numerical aperture were used and an adaptive correlation algorithm, with a final interrogation area size of 16 pixels × 16 pixels, was applied. A spatial resolution of 20.6 × 20.6 μm was achieved

using a window overlap of 50% in stream-wise and lateral directions, and the depth of correlation was 42.4 µm.

The water flow in the channel was generated with a programmable pump, consisting of two syringes (WPI AL4000, World Precision Instruments) and ensuring a maximum flow rate of 114.5 ml/min. The pulsatile flow was created with an OB1 MK3 microfluidic flow control system provided by Elveflow. Moreover, 1.0-µm-diameter fluorescent particles (Invitrogen) with a specific gravity of 1.05 and excitation and emission wavelengths of 535 nm and 575 nm, respectively were used.

The principal scheme of image processing is presented in Fig. 4. Two successive images of particles are recorded within known time interval Δt. Then particle image fields are divided into interrogation regions of a certain size where cross-correlation function is calculated to determine the most probable local displacement. The velocity of a fluid is calculated by dividing the measured displacement, Δx, by the time delay:

$$v_x = \frac{x_{t+\Delta t} - x_t}{\Delta t} = \frac{\Delta x}{\Delta t}. \tag{2.1}$$

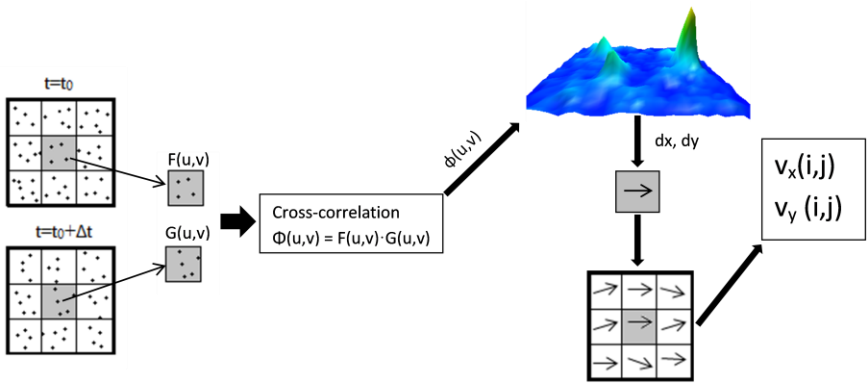

Fig. 4. Principal scheme of µPIV images processing

2.2. Uncertainty analysis

The uncertainty of velocity measurements using µPIV is determined by comparing mean velocity values, calculated according to the syringe pump readings, and measured velocity profiles. Furthermore, uncertainty is determined by examining the conformity of the measured velocity profiles to the known consistent patterns of velocity distribution in laminar and turbulent flow regimes. Such analysis revealed that the expanded uncertainty of velocity measurement does not exceed 6.8 %. The main components of the total standard uncertainty budget were the flow rate measurement (≤ 0.6 %), the channel cross-section area

determination (≤ 2.8 %), and the repeatability evaluation, up to nine measurement repetitions (≤ 1.9 %).

There are three main components of uncertainty for recirculation zone length. The exact reattachment location could not be determined owing to the limited spatial resolution of μPIV. Moreover, to obtain images with a high spatial resolution and low measurement depth, high-magnification objective lenses were used. Therefore, the field of view becomes extremely small to cover the entire cavity at once, and images of separate parts of the cavity were taken and combined. Recirculation zone length was determined according to the location where the reattached flow split into the upstream and downstream flows. This location slightly changes over time; therefore, the reattachment point was determined for every image pair. This variation was minimal in the laminar flow regime, and the repeatability did not exceed 2.3 %. In the turbulent flow regime, the reattachment point fluctuated more and repeatability reached 8.9 %. The total expanded uncertainty of the reattachment point evaluation did not exceed 15 %.

2.3. Numerical methods

The commercially available CFD package *Ansys Fluent* and RSM-BSL turbulence model for 2D and 3D computation of the time-averaged flow parameters were used. Furthermore, the LES model was used to receive images of the dominant time-dependent flow vortices. The channel geometry was modeled using *DesignModeler*. After mesh refinement along the channel boundaries, the ratio of minimal and maximal node size to the height of the channel was 0.0015 and 0.006, respectively. Grid independence studies showed that the solution is not affected by a further increase in the number of cells. Mesh, which is close to the walls, has an increasing number of cells (Fig. 5). Fifteen cell layers were used to resolve the boundary layer with a minimum cell height being in the order of 10^{-6} m. Mesh was imported into *Ansys Fluent* solver and SIMPLEC solution algorithm, together with second-order upwind discretization schemes, was used in the simulations. A convergence criterion was set to 10^{-6} for all variables. For LES simulations, the time step size was set to 10^{-5} s with 40 iterations per time step.

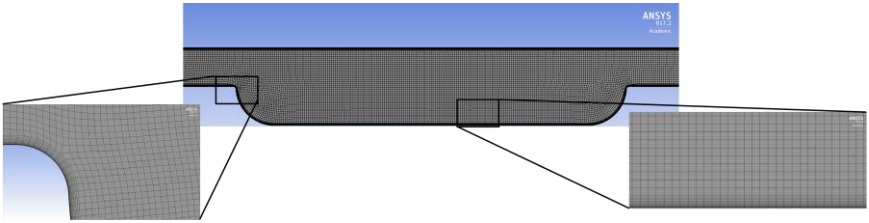

Fig. 5. CFD geometry and grid structure at the bottom of the cavity and around the cavity edge. Note: For the sake of visibility presented grid contains a smaller amount of cells than used for computation

3. RESULTS AND DISCUSSION

3.1. Flow in transitional and closed-type cavities

Experimentally measured relative recirculation zone length values are presented in Fig. 6. As can be seen, recirculation zone dynamics depend on the type of cavity and channel expansion ratio. Also, a pattern is different depending on which parameter Re is based. In the case of the transitional-type cavity with low channel expansion ratios, recirculation zone length curves have breakpoints in the transitional flow regime. In the case of closed-type cavity peak values of relative recirculation zone length are reached at different Re_{Dh} values. Also, the sharp peak of x_r/h_1 disappears in the case of a high channel expansion ratio. The causes of the mentioned phenomenon are explained in the following chapter, starting with the investigation of flow over the transitional-type cavity.

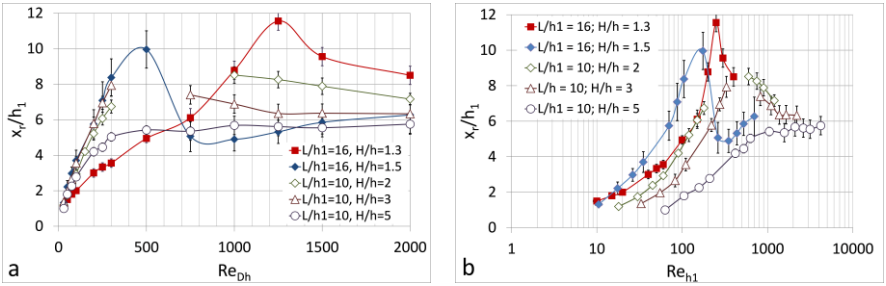

Fig. 6. Experimentally measured relative recirculation zone length values in different types of cavities depending on a) Re_{Dh} and b) Re_{h1}

3.1.1. Recirculation zone length dependence on Re_{Dh}

The reattachment point locations on the bottom of the cavity and the averaged local velocity vector maps, obtained by μPIV, are shown in Fig. 7 and Fig. 8, respectively. As it follows from experimental flow field data, flow separation starts when Re_{Dh} reaches 30 (Fig. 8a), as the corners of the cavity are rounded and the separation does not appear at $Re_{Dh} < 30$. As Re_{Dh} increases from 30 to 300, the relative length of the recirculation zone (x_r/h_1), bounded by the flow reattachment to the cavity bottom, increases in a nearly linear manner from $x_r/h_1 = 1.1$ to $x_r/h_1 = 6.9$ (Fig. 7).This lengthening pattern is determined by the small spreading rate of the mixing layer between the separated and recirculation flows in the laminar flow regime. In this Re_{Dh} range recirculation zone consists of a single stable vortex. Also, at $Re_{Dh} = 240$, the signs of vortex formation, in front of the forward-facing step, appear and the vortex becomes visible at $Re_{Dh} = 300$ (Fig. 8b).

For the investigated case, the values $Re_{Dh} = 300$ and $x_r = (0.6–0.7)L$ can be considered marginal for conventional flow reattachment. This phenomenon was

also observed by Esteve, Reulet, & Millan (2000) in turbulent flow over a rectangular cavity with similar relative dimensions. For Re_{Dh} ranging from 320 to 1000, the averaged velocity vector field within the cavity shows the formation of a quite stagnant closed recirculation loop without reattachment (Fig. 8c, see also velocity profiles in Fig. 12c). The zero-velocity line, dividing the downstream and upstream flows, approaches the cavity lid and positions itself parallel to the cavity bottom. From a topological point of view, it is possible to discern information from the saddle between two sub-loops having a dumbbell-like shape, which is typical for interfaces between dual vortices (Gurcan, 2003).

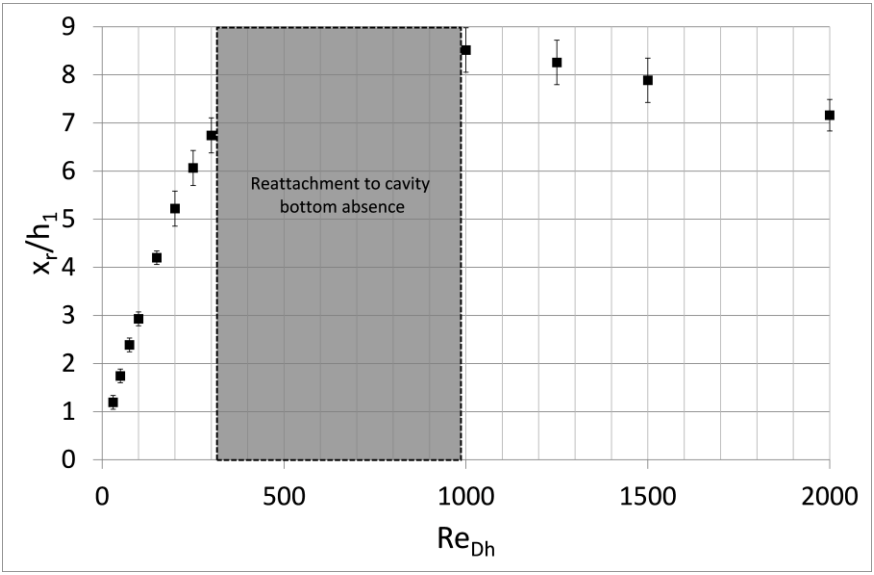

Fig. 7. Dependence of the recirculation zone length on Re_{Dh} for transitional-type cavity ($L/h_1 = 10$, $H/h = 2$)

However, such topology is disrupted by the instabilities related to the transition from laminar to turbulent flow regimes in the channel. For $Re_{Dh} \approx 700–800$, the temporal formation of individual vortices pathways is observed in instantaneous flow fields without any signs of reattachment. Only at $Re_{Dh} = 1000$, the flow reattachment to the bottom of the cavity is observed again at $x_r/h_1 = 8.5$ (Fig. 8d). With further increase of Re_{Dh} up to 2,000, the recirculation zone length decreases at descending rate to $x_r/h_1 = 7.2$, suggesting that this ratio gradually moves to a consistent asymptotic level, which was also observed by other authors for turbulent flow in channels with sudden expansion or obstacles (Fig. 2).

The averaged experimental results at $Re_{Dh} = 1{,}500$ (Fig. 8e) show the appearance of dynamical flow structures in the recirculation zone behind the

backward-facing step of the cavity. Such phenomena in a turbulent flow regime may be substantiated by the systematically detaching and reoccurring structure of vortices in this zone. It can be more clearly demonstrated by the time-dependent analysis of vortices generation and their topology by comparing the experimental and numerical simulation data presented in the following sections.

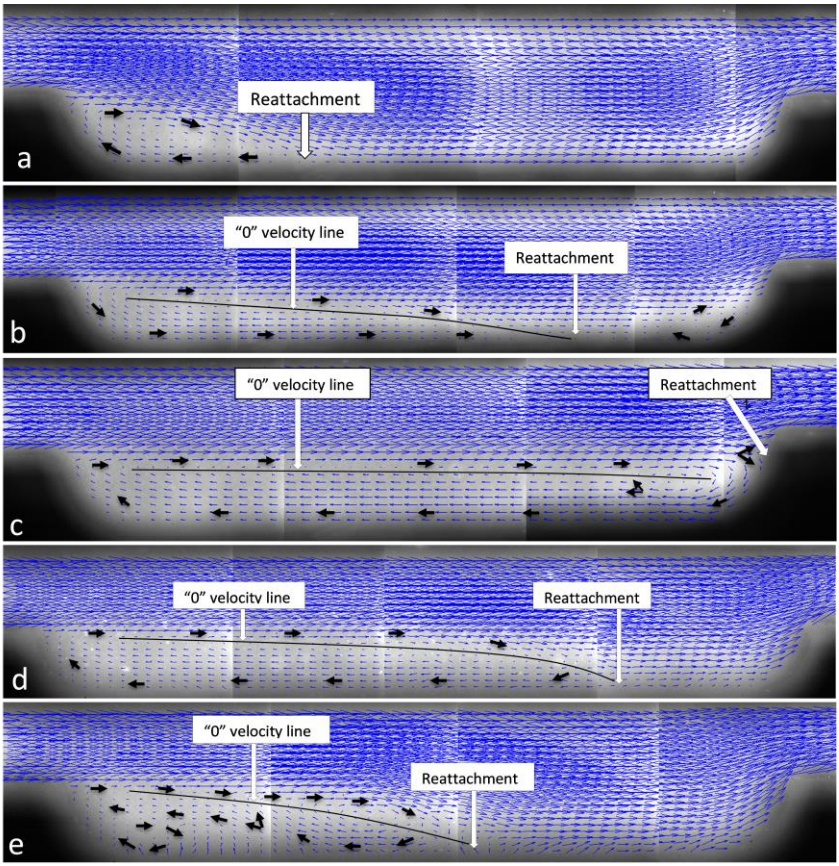

Fig. 8. Experimentally measured time-averaged velocity vector fields in transitional-type cavity ($L/h_1 = 10$, $H/h = 2$) at Re_{Dh}: a) 100 b) 300 c) 800 d) 1000 and e) 1500

3.1.2. Inner recirculation zone structure

The purpose of this section is to reveal time-dependent changes of the inner flow structure, which determine the values of time-averaged flow parameters. It is done by presenting a qualitative analysis of flow fields at different flow regimes.

Figs. 9 and 10 provide the instantaneous flow fields by applying the LES model in transitional and turbulent flow regimes. The time step between the presented LES images was 4×10^{-4} s and the period of the cycle was 0.002 s.

In the laminar flow regime, experimental and computational results show a single stable vortex elongated downstream from the backward-facing step. As the Reynolds number increases, at Re_{Dh} = 320–1000, the reattachment flow is lifted from the cavity bottom and reattachment can no longer be observed (Fig. 8c). In this range, the experimental and simulation results provide similar images (Figs. 9a and b) of the flow field, consisting of an elongated stagnant recirculation loop (1) and an intensive vortex (2) near the forward-facing step with a saddle point (3) between them. While increasing Re_{Dh}, the mixing layer (4) instabilities grow strongly and the contours of vortices along the cavity appear. Eventually, instabilities in the mixing layer grow to such a degree that the vortex at the forward-facing step starts to be periodically pushed from the cavity and immediately replaced by a similar one.

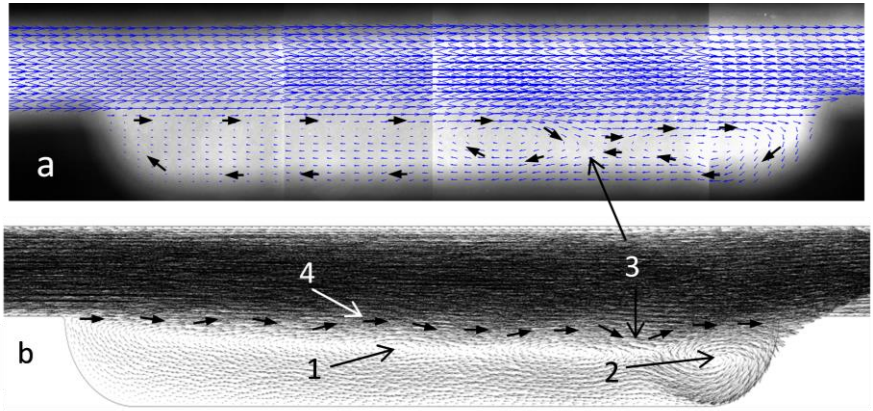

Fig. 9. Comparison between instantaneous experimental a) and computational b) velocity fields at Re_{Dh} = 800: 1–elongated stagnant recirculation loop, 2–the vortex at forward-facing step, 3–saddle zone, 4–mixing layer on the interface between the channel and cavity flows

After approaching a fully developed turbulent flow regime, the flow structure in the cavity undergoes drastic changes and becomes similar to the flow structure typical for the separated flow. Despite the continual formation of vortices, their separation, and driftage owing to the flow, stable periodical regeneration of vortices takes place and averaged flow parameters can be consequently identified. The simulation results presented in Fig. 10 show the following sequence of events during a single period of dynamical structures lifetime:

- formation of the primary vortex (1) (Fig. 10a) is predetermined by high adverse pressure gradient at the inlet of the cavity and intense interaction between separated and recirculating flows. These force the flow to reattach to the bottom of the cavity. The size of the vortex in turbulent flow is determined by the geometry of the cavity and it cannot be higher than the cavity depth;
- when the critical size of the primary vortex (1) is reached, the vortex is detached from the backward-facing step and a new vortex (2) begins to form (Fig. 10b);
- owing to the interaction between the separated shear layer and the secondary vortex (2) near the edge of the backward-facing step, a high-intensity tertiary vortex (3) begins to form (Fig. 10c). This vortex grows rapidly and occupies the position of the primary vortex (Fig. 10d);
- the development of a vortex on the upper channel wall has a strong impact on flow reattachment to the bottom of the cavity, which in this case is located at $x_r/h_1 = 5.8$.

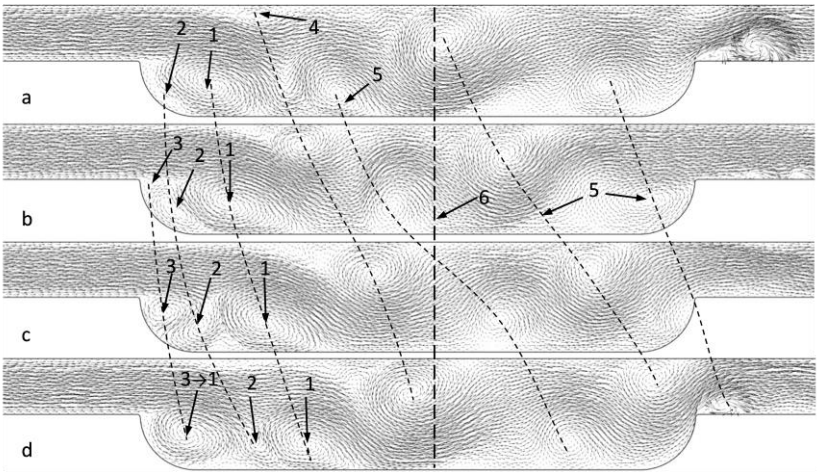

Fig. 10. Instantaneous simulated velocity flow fields in a turbulent flow regime at Re_{Dh} = 1,500: 1, 2, 3 – dominant vortices in recirculation zone, 4 – vortex on the upper wall of cavity, 5 – pathways of vortices (1) and (4) downstream of the reattachment, 6 – averaged position of the reattachment according to experimental data (Fig. 7)

It is also evident that vortices (1–4), up to the reattachment point, form a compact and definite system. Beyond the reattachment point, flow consists of vortices (1) and (4) moving toward the forward-facing step of the cavity. Similar simulation, performed at Re_{Dh} = 3,200, showed that the inner structure of vortices remains the same without noticeable changes. Similar vortex structures

have also been observed by Spazzini et al. (2001), Dejoan, Jang, & Leschziner, (2005).

3.1.3. Comparison of time-averaged experimental and computational results

As the numerical simulations, based on the solution of RANS equations and various turbulence models have significant applications in practice, further the comparison between such simulations, using the RSM-BSL turbulence model, and experimental results are presented. This turbulence model was selected as it is a physically complete turbulence model used for complex flow and provides a good agreement with experimental results in many practical cases.

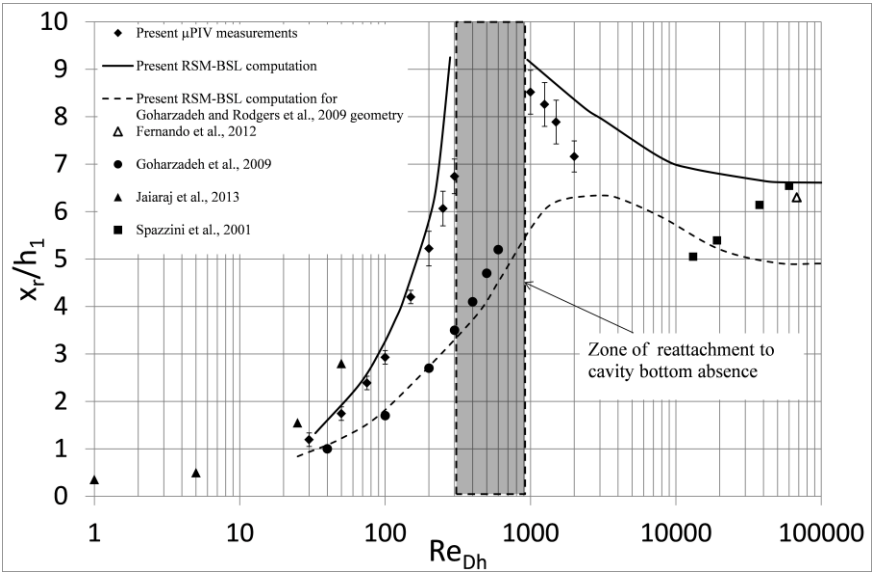

Fig. 11. Comparison between experimental and computational values of the reattachment length as a function of Re_{Dh}

Fig. 11 presents the comparison between the experimental and computational results of our study, as well as experimental data from other studies. The location of the reattachment point in simulated flow fields was determined as the minimum value of wall shear stress on the bottom of the cavity. For comparison, the values obtained for abrupt expansions of channels with rectangular cross-sections were chosen (Fernando et al., 2012; Jayaraj et al., 2013; Spazzini et al., 2001). In these cases, the aspect ratio of the channels varies from $z/h = 2.7$ to $z/h_1 = 35$ and the expansion degree $H/h \approx 1.3–2$. Thus, in our

study, values of z/h = 5 and H/h = 2 falls within these ranges. Additionally, data from Goharzadeh & Rodgers (2009) were used to verify the computational model in a channel where the two-dimensional flow is realized.

This comparison, while considering the data analysis obtained from different geometries, Fig. 1, confirms that with an increasing Re_{Dh} in a laminar flow regime, the recirculation zone length linearly increases until the transition from laminar to turbulent flow is reached. In the turbulent flow regime, the variation in the recirculation zone length becomes less dependent on the geometry of the channel expansion and Re_{Dh}. When $Re_{Dh} > 10^4$ (L. Chen, Asai, Nonomura, Xi, & Liu, 2018), the relative recirculation zone length remains in the range $x_r/h_1 \approx 6–8$ for reasons related to the above-mentioned formation of a periodical regeneration system of vortices, whether it is the flow over the single-step or the cavity.

However, some deviations occur while approaching the transition to a turbulent flow regime. As can be seen in Fig. 11, 2D computed recirculation length values in the transitional flow regime exceed experimental ones, obtained in our study, for flow over the cavity. The data from Goharzadeh & Rodgers (2009) obtained only at Re_{Dh} = 40–600 for flow over the backward-facing step, deviate less from the computed results. However, in fully turbulent flow, computed results approach the experimental results of other studies (Fernando et al., 2012; Spazzini et al., 2001).

These deviations are confirmed by a comparison between the averaged experimental and simulated velocity profiles, at different relative distances x/h_1 from the backward-facing step; see Fig. 12. For the laminar flow regime (Figs. 12a and 12b), experimental and computed velocity profiles satisfactorily coincide over the entire length of the cavity. The backward flow velocity is the highest near the backward-facing step, gradually decreases along the cavity and reaches no more than 10% of the velocity of the main flow. Because of the channel cross-section expansion, the velocity along the cavity decreases until it takes its smallest value at the reattachment point. For the transitional flow regime (Fig. 12c), the flow reattachment point is not observed and the recirculation zone remains throughout the cavity. The magnitude of the backward flow increases along the cavity length and reaches its maximum at $x/h_1 \approx 7$ and $y/h_1 \approx 0.1$. The transition to the turbulent flow regime is confirmed by the flattened velocity profiles of the main flow above the cavity (Fig. 12d). On the front part of the cavity, after the reattachment point, the shape of the velocity profile is irregular owing to the influence of the forward-facing step and the high Re number. In the case of Re_{Dh} = 1,500, the last stage of transition to turbulent flow, downstream of the reattachment point, computed velocity profiles are parabolic in the main flow and have slightly higher velocity values compared to the experimental ones.

By evaluating the nature of the deviation pattern variation between the computed and experimental results, it can be stated that discrepancies are

determined by at least two factors: the two-dimensional simulation of flow over the cavity and the limitation of the RSM-BSL turbulence model in the case of flow separation. First, a calculation of the three-dimensional flow must be performed, which was not possible in this study owing to the lack of computational resources available. Moreover, there are satisfactory arguments to conclude that the RSM-BSL model underestimates the turbulent energy generation, induced by flow instabilities and separation phenomena. Therefore, a more detailed investigation is required of the turbulence CFD models for computing reattaching flows.

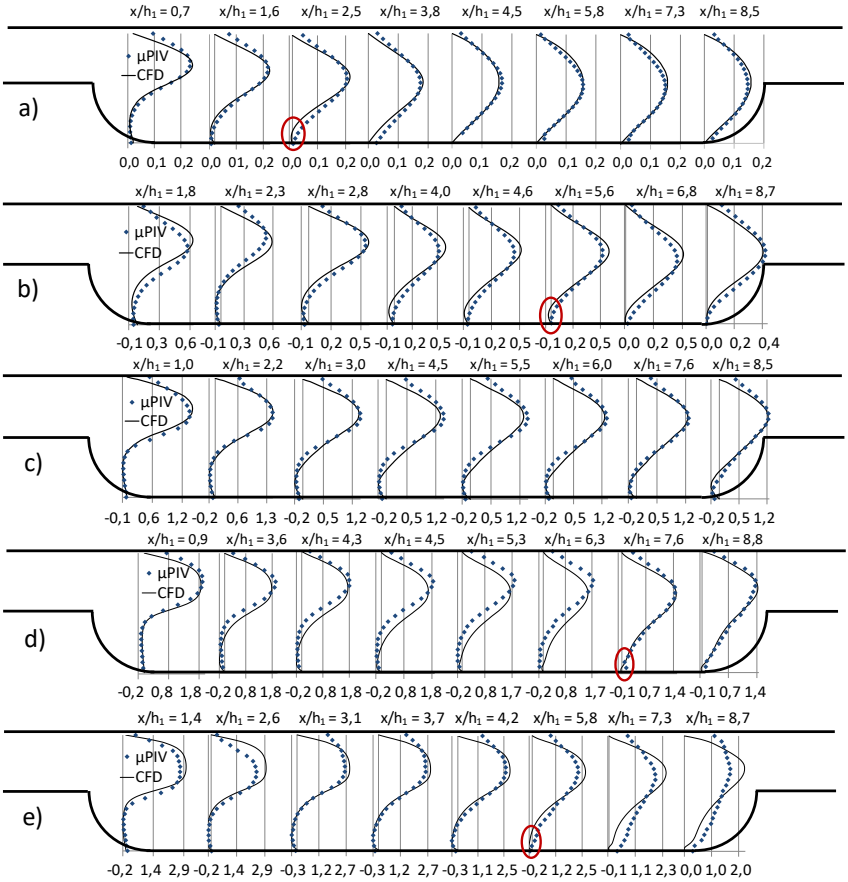

Fig. 12. Comparison between experimental and simulated velocity profiles at different locations behind the backward-facing step at Re_{Dh}: a) 100, b) 300, c) 800, d) 1000 and e) 1,500. Note: Circles indicate the reattachment point according to the experimental results

3.2. Parametrical analysis

In this chapter, cavity geometrical parameters were changed in order to investigate their influence on recirculation zone length dynamics.

3.2.1. The influence of cavity relative length on recirculation zone dynamics

Recirculation zone structure, as well as the dynamics of recirculating flow length, depends on the type of cavity, which is determined by the cavity length-to-depth ratio (L/h_1). Experimental and numerical results of relative recirculation zone length (x_r/h_1) at a wide range of Re_{Dh} and cavity length-to-depth ratios ($4 \leq L/h_1 \leq 36$) are presented in Fig. 13. Other cavity parameters (cavity depth h_1, expansion ratio H/h) are kept constant. In this case, all three types of cavities (open, transitional and closed-type) are covered.

In the case of $L/h_1 = 4$, the flow in the cavity is open-type, and no attachment to the bottom wall of the cavity is observed. Reattachment to the bottom wall of the cavity is observed when $L/h_1 = 6$ is reached. However, the shear layer attaches to the bottom wall only at the low values of $Re_{Dh} \leq 85$. Exceeding this value the flow structure in the cavity becomes open-type in the remaining Re_{Dh} range. After increasing cavity length to $L/h_1 = 8$, cavity becomes transitional-type and remains until $L/h_1 = 12$.

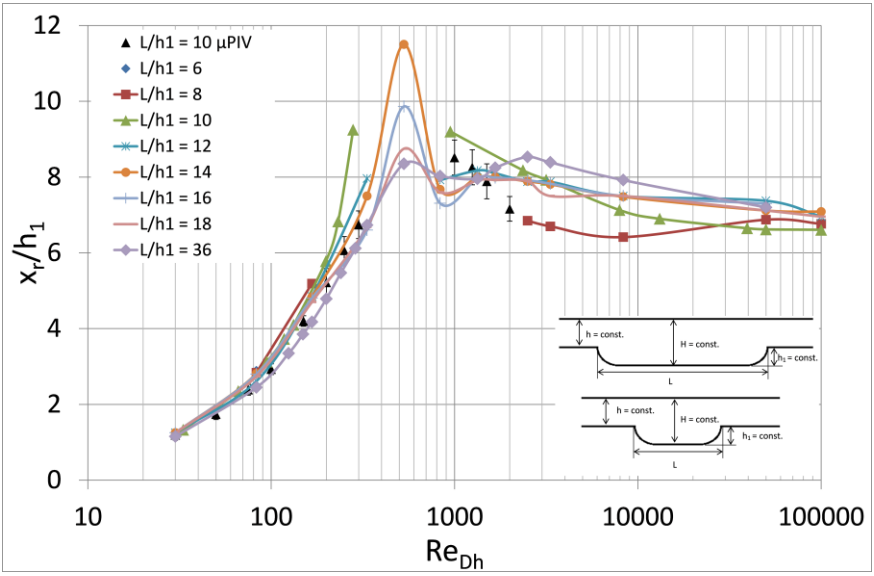

Fig. 13. Dependence of relative recirculation zone length on Re_{Dh} for different relative lengths of cavities

After $L/h_1 = 14$, the cavity is closed-type, and shear layer attachment to the bottom wall of the cavity occurs in the whole investigated Re_{Dh} range. As can be seen from Fig. 13, the peak value of relative recirculation zone length decreases as relative cavity length increases. x_r/h_1 reaches asymptotical value as relative cavity length increases, and the influence of the forward-facing wall of the cavity is negligible. Flow structure in the cavity becomes similar to flow over the backward-facing step. Also, in the cases of transitional and closed-type cavities, in the fully developed turbulent flow regime relative recirculation zone length reaches asymptotical value independent of the length of the cavity.

3.2.2. Channel expansion ratio influence to recirculation zone dynamics

In Fig. 14 and Fig. 15 dependence of recirculation zone length on Re_{Dh} for different channel expansion ratios but constant cavity depth and length values are presented. Two separate cases of transitional ($L/h_1 = 10$) (Fig. 14) and closed ($L/h_1 = 16$) (Fig. 15) type cavities are investigated. In both cases, recirculation zone length increases as channel expansion ratio increases at the same Re_{Dh} value (except the case of $H/h = 5$). In the case of the transitional-type cavity (Fig. 14), shear layer reattachment at turbulent flow regimes occurs at higher Re_{Dh} values as channel expansion ratio decreases. In the case of the closed-type cavity (Fig. 15), the peak value of relative recirculation zone length decreases as channel expansion ratio increases. Higher channel expansion ratio leads to a faster growth of the separated shear layer. It forces the shear layer to attach to the bottom wall of the cavity at a shorter distance from the backward-facing wall of the cavity. Also, the peak value of recirculation zone length occurs at higher Re_{Dh} as channel expansion ration decreases. This shift indicates that the transition to a turbulent flow regime occurs at higher Re_{Dh} values as channel expansion ratio decreases.

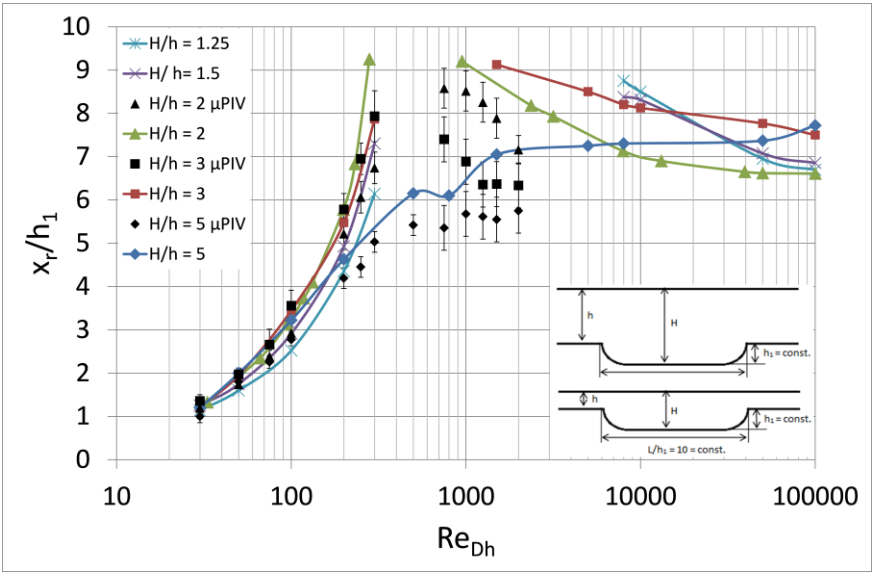

Fig. 14. Dependence of relative recirculation zone length on Re_{Dh} for different H/h values in the case of the transitional-type cavity ($L/h_1 = 10$)

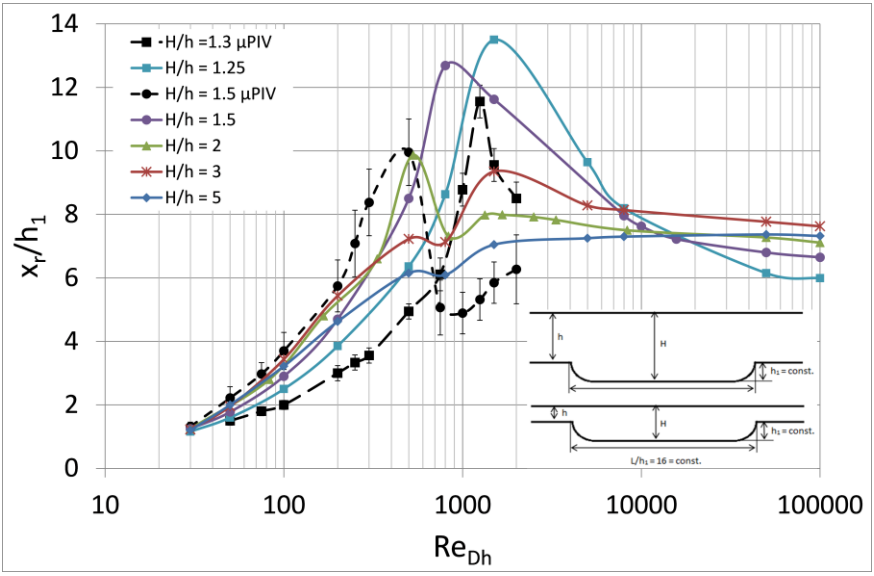

Fig. 15. Dependence of relative recirculation zone length on Re_{Dh} for different H/h values in the case of the closed-type cavity ($L/h_1 = 16$)

It should be noted that the case of H/h = 5 for both types of cavities has similar values in the whole range of investigated Re_{Dh}. Also, in the case of the transitional-type cavity (Fig. 14), shear layer attachment to the bottom wall of the cavity is persistent in the whole Re_{Dh} range, while absent of shear layer attachment in transitional flow regime is typical for such type of cavity.

In Fig. 16 relative recirculation zone length values depending on channel expansion ratio at different Re_{Dh} are presented. In general, recirculation zone length increases as the channel expansion ratio increases from 1.25 to 2. In the case of laminar flow regime peak values of x_r/h_1 are reached when H/h = 2. In the case of transitional flow regime, peak values are in the range of $1.5 \leq H/h \leq 2$. In the turbulent flow regime, the peak value is reached when H/h = 3. The fastest-growing rate of x_r/h_1 is observed in laminar (at higher Re values) and transitional flow regimes, while the slowest rate is at low Re values and in turbulent flow regime. Further increasing H/h, relative recirculation zone length values decrease. The rate of decline is fastest in the transitional flow regime and insignificant in laminar and turbulent flow regimes.

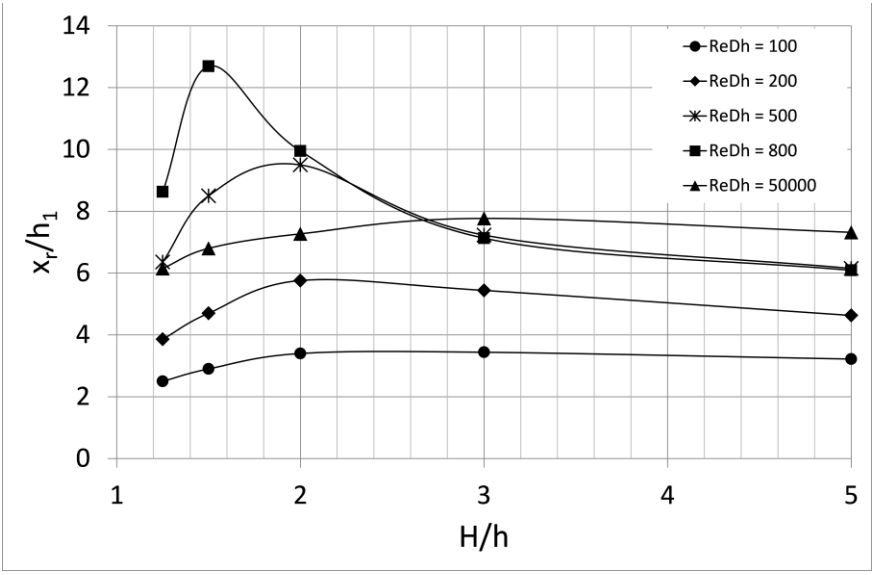

Fig. 16. Dependence of relative recirculation zone length on H/h at different Re_{Dh} values in the case of the closed-type cavity ($L/h_1 = 16$)

3.2.3. Comparison of relative recirculation zone length dependence on Re_{Dh} and Re_{h1}

So far, hydraulic diameter D_h was chosen as the characteristic linear diameter for Reynolds number. Therefore Re_{Dh} determines the flow regime in the channel. However, as can be seen from the results presented, the dynamics of recirculation zone length also depend on the height of cavity h_1. For comparison, the case of L/h = 16 at varying channel expansion ratio is chosen (Fig. 15). Relative recirculation zone length values depending on Re_{h1} parameter are presented in Fig. 17. It can be seen that using Re_{h1} peak relative recirculation zone length values occurs at the same Re_{h1} value when $H/h \leq 2$. At higher values of H/h peak values of x_r/h_1 are slightly shifted to the higher Re_{h1} side. Also, as H/h value increases, x_r/h_1 decreases at the same Re_{h1} in the laminar flow regime. The reverse situation is observed in the turbulent flow regime. x_r/h_1 value increases as H/h increases in the same Re_{h1}.

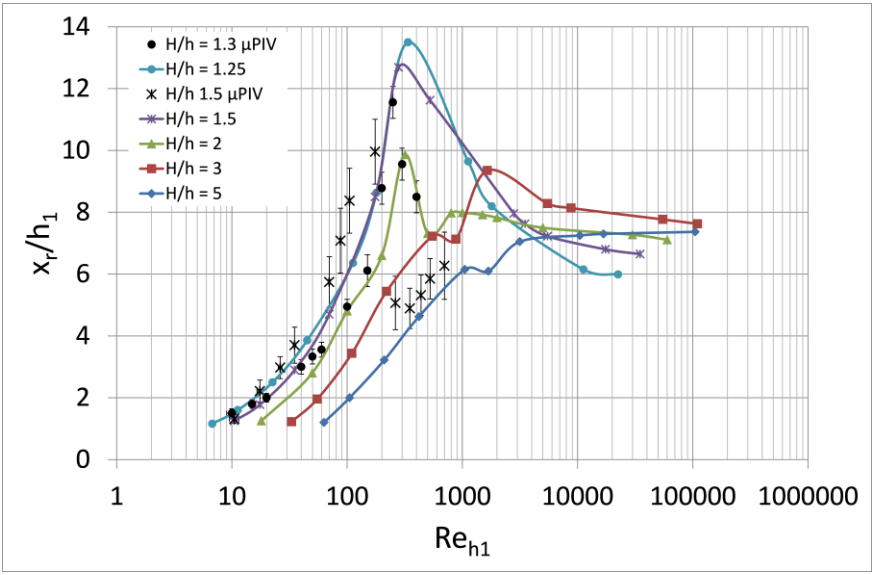

Fig. 17. Dependence of relative recirculation zone length on Re_{h1} for different H/h values in the case of the closed-type cavity ($L/h_1 = 16$)

Such distribution of relative recirculation zone length is not suitable for practical purposes. As can be seen from Figs. 14 and 15, channel expansion ratio H/h influences the dynamics of recirculation zone length. Therefore, an additional parameter can be introduced – $(H/h)(x_r/h_1)$. This parameter is also used by Tihon, Pěnkavová, Havlica, & Šimčík (2012) in analysing the flow over the backward-facing step in the laminar flow regime. This distribution is

presented in Fig. 18. In this case, values of relative recirculation zone length are distributed on a single trend in the laminar flow regime. Peak values still occur at the same Re_{h1} value, when $H/h \leq 2$. In turbulent flow regime value of $(H/h)(x_r/h_1)$ is directly proportional to channel expansion ratio (H/h) component.

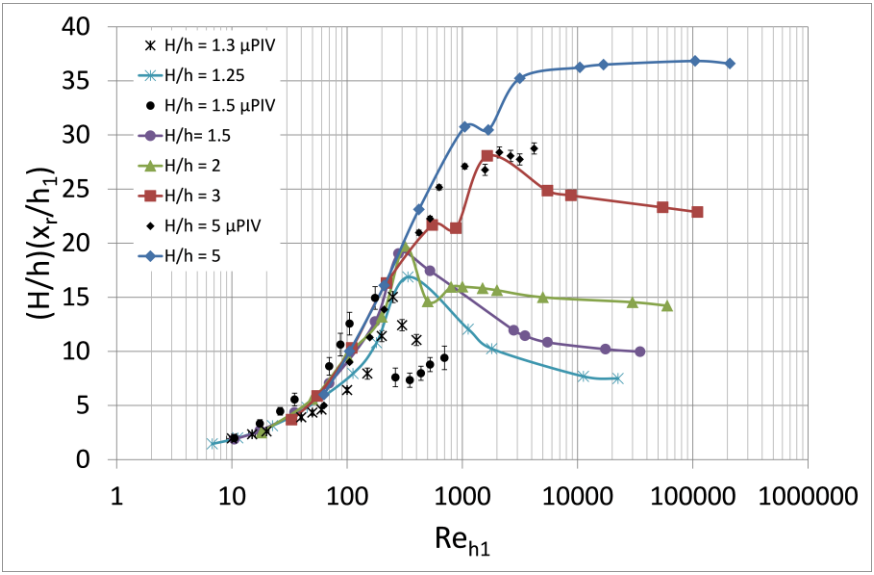

Fig. 18. Dependence of relative recirculation zone length multiplied by channel expansion ratio on Re_{h1} for different H/h values in the case of the closed-type cavity ($L/h_1 = 16$)

3.2.4. Influence of channel expansion ration to reattachment length dynamics

From the physical point of view, it is more expediently to relate channel expansion ratio with the expansion of the mixing layer formed due to the interaction of separated shear layer with the recirculating flow behind the backward-facing wall. It is well known that the growth rate of the separated shear (mixing) layer is determined by the transversal velocity pulsation component and can be estimated as:

$$d = \frac{v_1 - v_2}{|v_1| + |v_2|} x; \qquad (3.1)$$

here, v_1 – inflow stream velocity; v_2 – flow in cavity velocity; x – distance from the inlet to the cavity. In our case, we have the asymmetric spreading of flow entering the cavity. v_2 value is chosen as the mean velocity in the cavity, which decreases $(h/H)^2$ times compared to mean velocity in the channel before entering

the cavity. The dependence of the separated shear layer spreading rate is presented in Fig. 19.

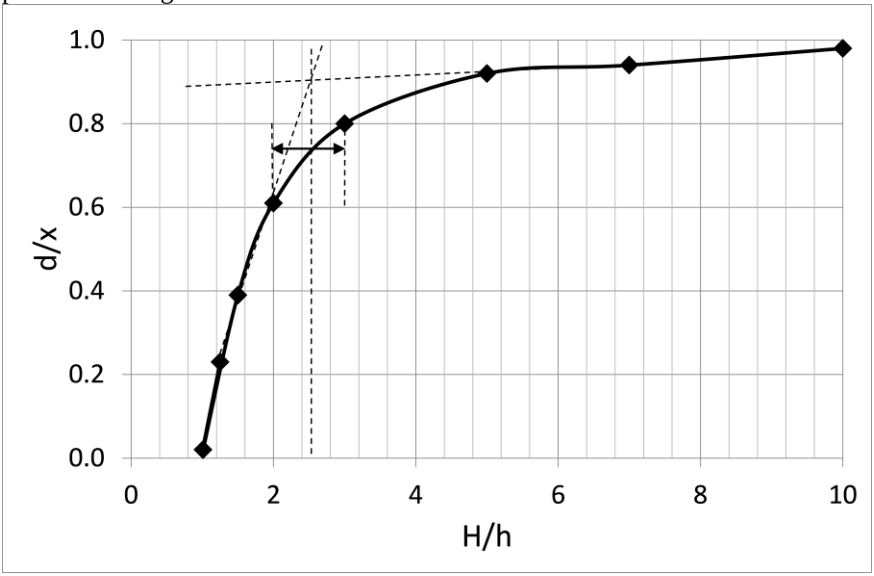

Fig. 19. Dependence of spreading rate of mixing layer in the cavity on channel expansion ratio

As can be seen from Fig. 17, distinct peaks of reattachment length at the transition from laminar to turbulent flow regime are observed only when $H/h \leq 2$. Further increasing Re_{Dh} relative reattachment length decreases and reaches an asymptotical value in a fully developed turbulent flow regime. However, in the case of $H/h > (2–3)$ smooth reattachment length growth without a well-defined peak is observed (Fig. 17). It is apparent that the adverse pressure gradient in the cavity increases as the channel expansion ratio increases ($dp/dx > 0$). The adverse pressure gradient forces the shear layer to reattach to the bottom wall of the cavity at a shorter distance. Whereas, the mixing layer spreading rate increases as the channel expansion ratio increases. For this reason, shear layer reattachment occurs at a lower distance and relative reattachment length shortens as H/h increases. The influence of adverse pressure gradient and shear layer spreading rate becomes dominant in the cavity as it changes reattachment length pattern in the transitional-type cavity (Fig. 14, case of $H/h = 5$). The recirculation zone is stabilized by the high adverse pressure gradient and the laminar flow regime persists up to higher Re_{h1} (Fig. 17). Also, the influence of the forward-facing step becomes insignificant at high channel expansion ratios.

The turning point in Fig. 19 corresponds to the H/h value at which mixing layer spreading rate, as well as, dynamics of recirculation zone length changes its

pattern in the cavity. The turning point is in the range of H/h = 2–3. Also, as can be seen from Figs. 13, 14 and 17, relative reattachment length dependence on Re can be separated into two groups when H/h < 2 and H/h > 2. In the case of H/h < 2, defined peaks and higher values of maximum relative reattachment length are observed compared to the case when H/h > 2. When H/h > 2 (especially when H/h = 5) relative recirculation zone length monotonically increases until the asymptotical value at a turbulent flow regime is reached.

3.2.5. Relative recirculation zone length scaling

While comparing the data presented in Figs. 14–15 and Figs. 17–18 it is evident that parameter Re_{h1} is more suitable for analysis of recirculation zone length dynamics. Also, additional factor H/h can be used to fit data on a single trend line in the laminar flow regime. However, in the turbulent flow regime, parameter x_r/h_1 seems to be more convenient for the analysis of recirculation zone length dynamics.

In Fig. 20 dependence of recirculation zone length on Re_{h1} in the laminar flow regime is depicted on the left side of the graph. The data can be fitted to a formula:

$$\left(\frac{H}{h}\right)\left(\frac{x_r}{h_1}\right) = 0.35 Re_{h1}^{0.7}. \tag{3.2}$$

This relationship is strong in the case of low Re_{h1} values. The error is less than 12 %, when $Re_{h1} < 150$. For comparison, the relation for backward-facing step flow estimated by Tihon et al. is valid for Re < 200 with an error of less than 7 %. The differences of the used coefficient are determined by the differences in geometries and the presence of forward-facing step in the case of cavity flow.

On the right side of Fig. 20, the dependence of relative recirculation zone length on Re_{h1} in the case of a turbulent flow regime is presented. Since the recirculation zone length in the turbulent flow regime depends only on Reynolds number and cavity geometry does not influence the structure of the flow. The relation can be written as:

$$\left(\frac{x_r}{h_1}\right) = 7 + 50 Re_{h1}^{-0.55}. \tag{3.3}$$

This relation becomes stronger as Re_{h1} increases because at fully developed turbulent flow regime relative recirculation zone length reaches its asymptotical value which is in the range of 6 to 8 step heights. The recirculation zone breaks into the system of separate vortices after the transition to a turbulent flow regime. The mean location of vortices attachment does not longer depend on Re_{h1} and remains constant.

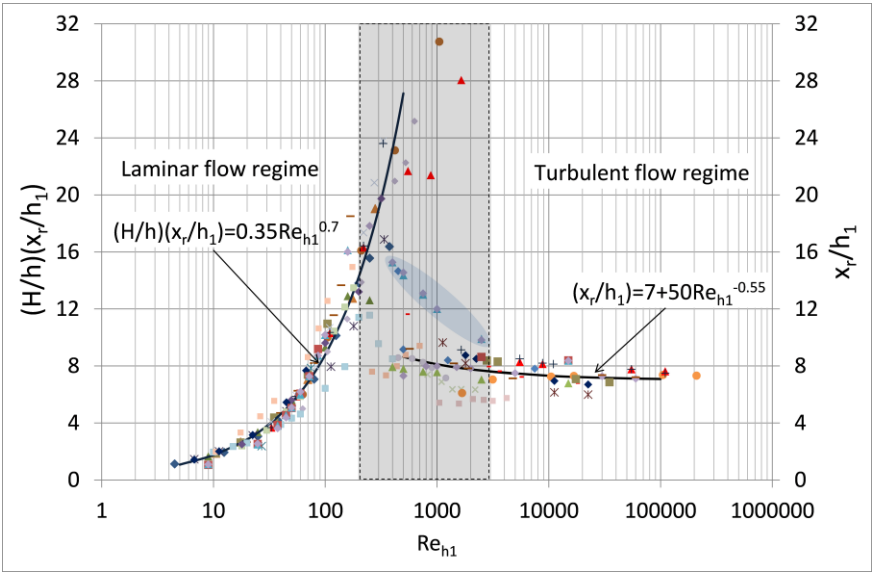

Fig. 20. Relation of recirculation zone length in laminar and turbulent flow regimes

As Re_{h1} increases in the laminar flow regime, as well as Re_{h1} decreases in turbulent flow regime, presented dependencies become weaker and scattering of points increases. It is due to the approaching of the transitional flow regime for which dependencies of recirculation zone length dynamics are not found. Different distribution is found for symmetrical channel expansion, which is a different case where cavities are on both sides of the channel. Cases where L/h = 10; 18 and 36 and H/h = 2 are presented in blue background in transitional flow regime. It is observed that these values decrease in a certain trend as Re_{h1} increases. The upper wall does not influence the flow structure in the cavity, hence the transition to turbulent flow regime is smoother. In laminar and turbulent flow regimes relations are the same as in asymmetrical channel expansion cases.

3.3. Flow in the open-type cavity

In previous chapters, flow structure and dynamics in transitional and closed-types cavities in which separated shear layer can reattach to the bottom wall of the cavity were analyzed. When the relative cavity length is decreased to the critical value of $L/h_1 < 6–8$, the separated shear layer bridges the cavity without reattachment to the bottom of cavity. In this chapter, a deep open-type cavity ($L/h_1 = 0.5$) was chosen to investigate the flow structure depending on the flow regime. In Fig. 21 a scheme of the investigated cavity is presented. Experimental measurements were performed at different x-z planes across the

center of the primary vortex. Also, a three-dimensional numerical simulation was performed.

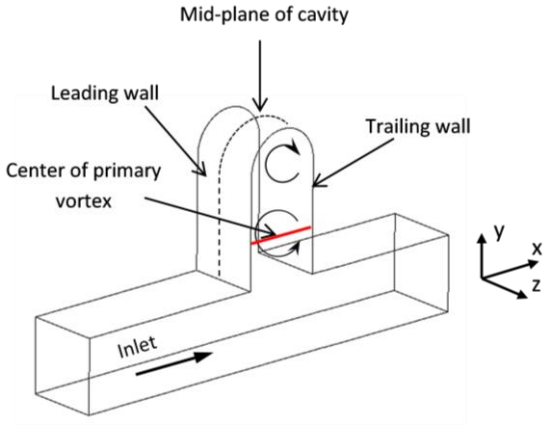

Fig. 21. Scheme of an investigated open-type cavity

3.3.1. Velocity distribution across the center of the primary vortex

Experimentally measured velocity distribution across the center of the vortex is presented in Fig. 22. Here the flow direction in the channel is from the left to the right. x/L = 0 corresponds to leading cavity wall and x/L = 1 – trailing cavity wall. Positive values of v_x correspond to flow direction in the channel. Also, positive values of v_y correspond to flow direction entering the cavity (from the cavity lid to the bottom) and negative values of v_y – flow directed from the cavity bottom to the lid.

As can be seen from Fig. 22, velocity distribution across the center of primary vortex depends on the flow regime. In the case of the laminar flow regime (Re_{Dh} = 100) maximum total velocity v is located near the trailing wall. The maximum positive v_x velocity component is located in the central part of the cavity and leading wall while negative velocity zones appear near the sidewalls and are stretched from the central part of the cavity towards the trailing wall. v_y velocity component distribution is similar to the case of total velocity since v_y contributes most to the total velocity (note the velocity values).

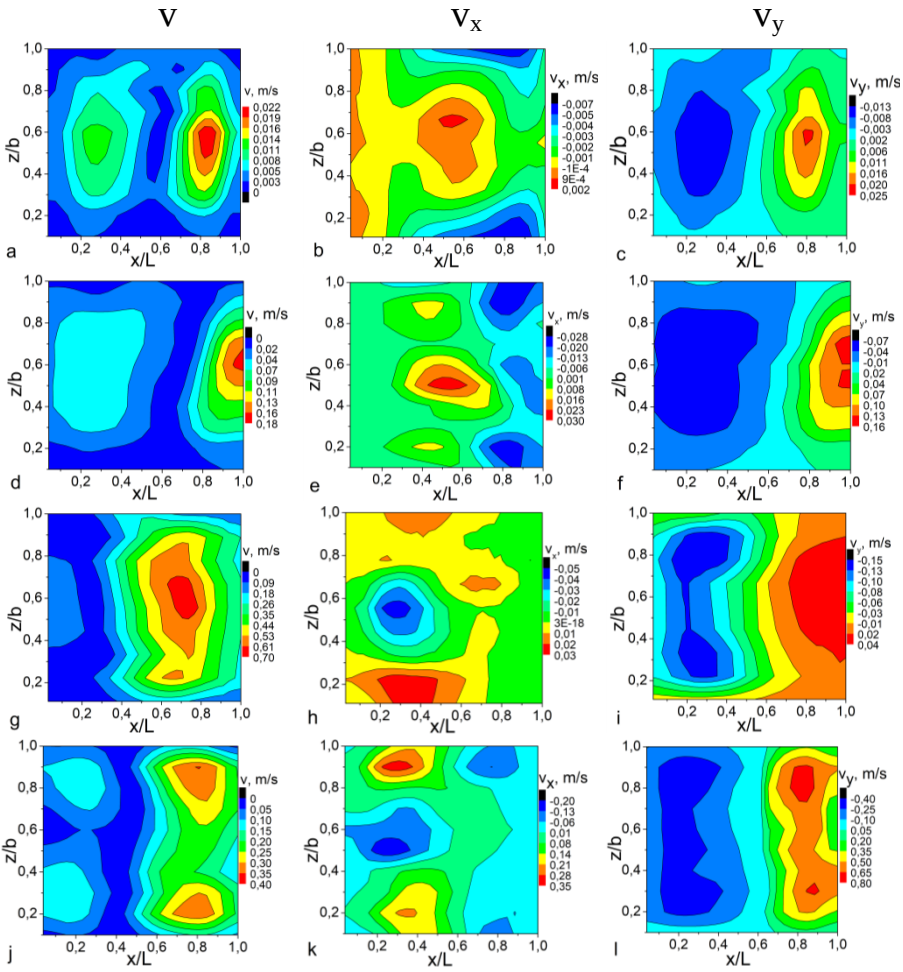

Fig. 22. Experimentally measured velocity scalar maps across the center of the primary vortex

Velocity profiles near the leading wall are measured at x/L = 0.2 and at x/L = 0.8 near the trailing wall for all cases. Flow in the cavity is laminar as it can be seen from measured and simulated velocity profiles having a parabolic shape in the case of total velocity (Fig. 23 a, d). Simulated velocity values are higher than the measured ones in all cases of v and v_x. Also, velocity near the trailing wall is about 1.8 times higher than near the leading wall. This ratio appears to be about the same for all Re numbers investigated.

After the transition to turbulent flow regime at Re_{Dh} = 3,000, experimental velocity scalar maps (Fig. 24) show flow division into two symmetrical structures in respect of cavity mid-plane. This velocity bifurcation is also observed in velocity profiles (Fig. 24 a, c, d and f) and it appears stronger in experimental measurements than in numerical simulation. As can be seen from Fig. 24a and Fig. 24d, in the case of experimental measurements two velocity peaks near sidewalls of the cavity, appear near leading and trailing walls. These measurements are in good agreement with numerical simulation except one case of total velocity near the leading wall (Fig. 24a), where an additional peak instead of a velocity minimum is observed.

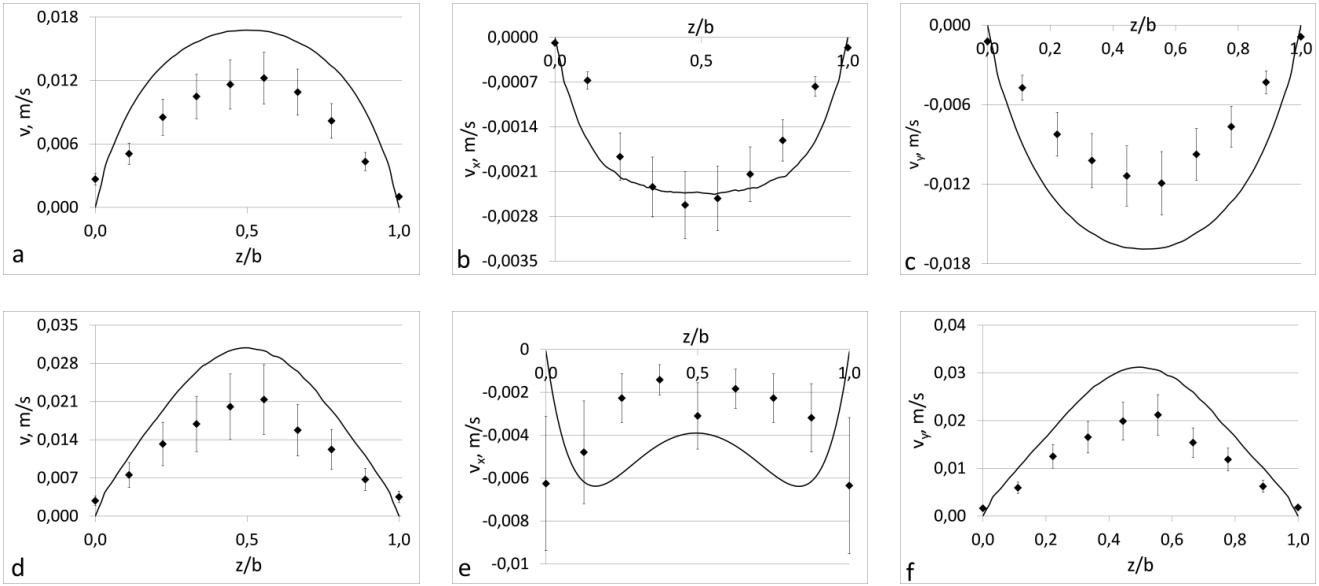

Fig. 23. Comparison of measured (dots) and simulated (lines) velocity profiles near leading (a, b, c) and trailing (d, e, f) walls at Re_{Dh} = 100: a and b – total velocity v; d and e – v_x component; c and f – v_y component.

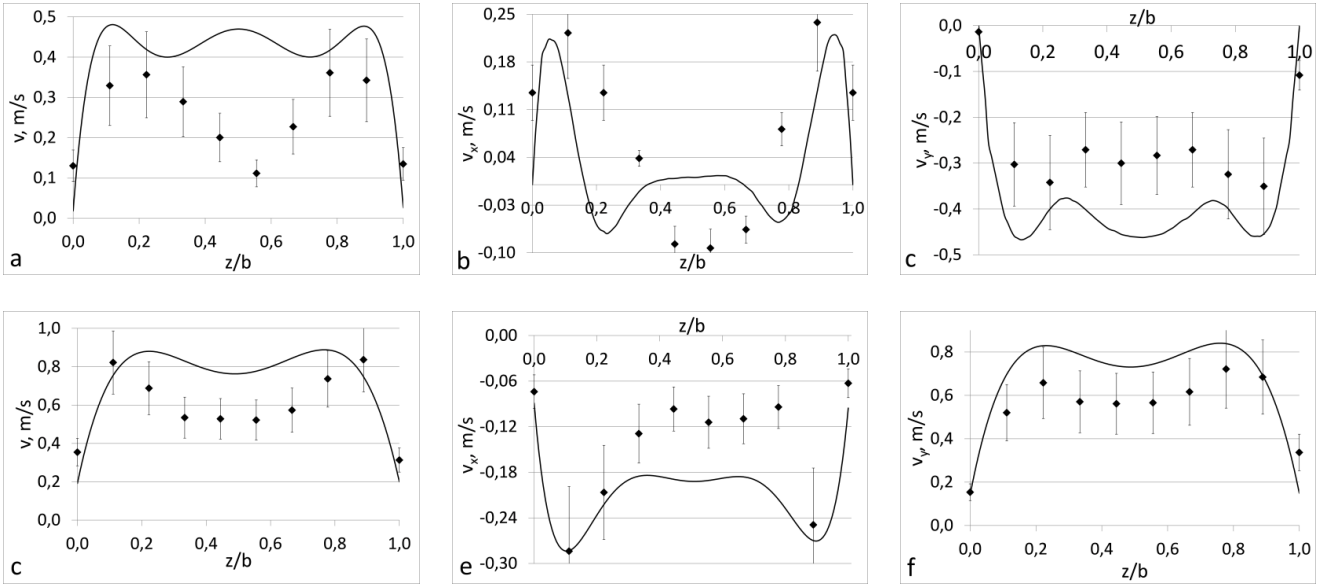

Fig. 24. Comparison of measured (dots) and simulated (lines) velocity profiles near leading (a, b, c) and trailing (d, e, f) walls at Re_{Dh} = 3000: a and b – total velocity v; d and e – v_x component; c and f – v_y component.

3.3.2. Flow structure across the center of the primary vortex

Streamlines at the x-z plane across the center of the vortex at different flow regimes are presented in Fig. 25 and velocity vectors at the same planes are presented in Fig. 26. After flow velocity in the channel increases up Re_{Dh} = 1000 corner vortices near the leading wall are formed. Flow structure is symmetrical with respect to the mid-plane of the cavity. Inward out-of-the-plane current formed in the center part of the cavity and directed towards the lid of the cavity is observed. While increasing Re_{Dh} this inward flow intensifies. The more significant volume of flow crosses the plane as it can be seen from a wider "V" shape structure at the center of the cavity (Fig. 26). As a result, vortices near the leading wall are squeezed into the corners. As Re_{Dh} increases, the gap of lower velocity flow between vortices also increases. At Re_{Dh} = 3000 (Fig. 25d) new velocity peak between vortices occurs, as can be seen in Fig. 24a.

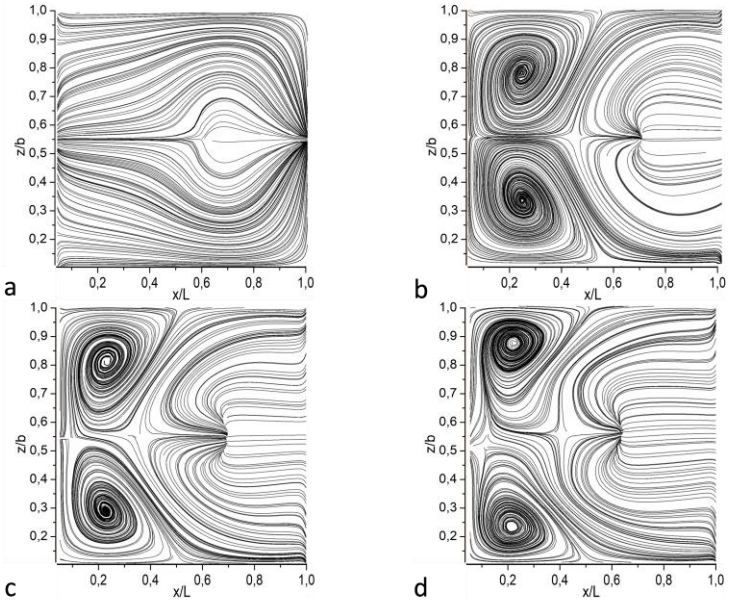

Fig. 25. Streamlines at x-z plane across the centre of vortex at Re_{Dh}: a) 100; b) 1000; c) 2000; d) 3000

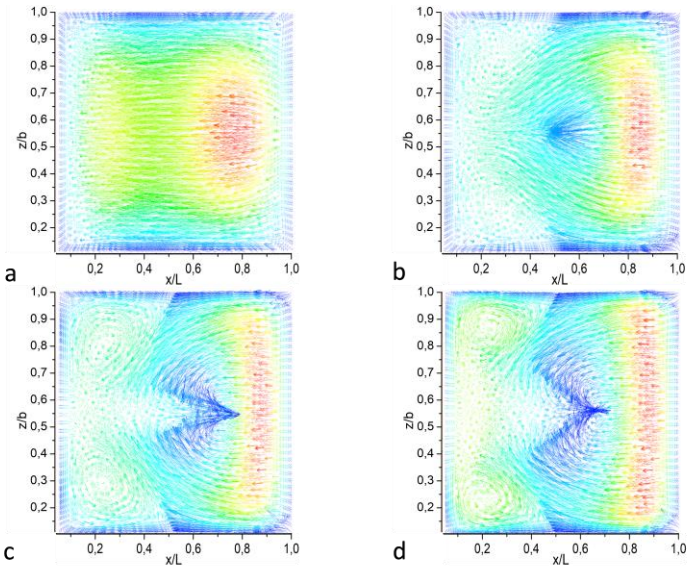

Fig. 26. Velocity vectors at x-z plane across the centre of vortex at Re_{Dh} a) 100; b) 1000; c) 2000; d) 3000

The scheme of flow streamlines at different measurement planes of the cavity is presented in Fig. 27. All flow fields are obtained by using three-dimensional numerical simulation. The present figure summarises the obtained results. Flow structure is symmetrical in respect of the cavity axis. Vortical flow in the deep open-type cavity at a turbulent flow regime ($Re_{Dh} > 1000$) is a system of counter-rotating vortices. Additional vortical structures are formed in the interception between the main flow in the main channel and recirculating flow in the cavity and between primary and secondary vortices in the cavity. Unfortunately, in this study, experimental measurement results alone are not sufficient to provide enough information on three-dimensional flow structure; therefore numerical simulation must be used.

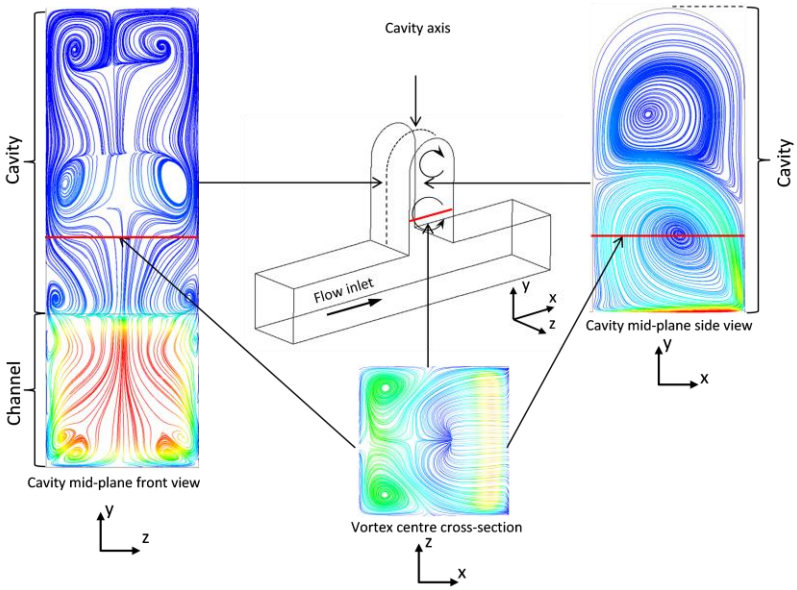

Fig. 27. Streamlines at different planes in the open-type cavity

3.3.3. Pulsatile flow in the open-type cavity

The pulsatile flow was chosen as an additional flow regime in the open-type cavity. In Fig. 28 ratios of velocities near the leading wall (v_{ld}) to trailing wall (v_{tr}) of the cavity are presented at different Womersley (Wo) numbers depending on Re_{Dh}. Velocities are measured across the center of the primary vortex. In most cases (Wo = 0.6–6.3 and stationary flow) peak value occurs at Re_{Dh} = 100. The peak values of v_{tr}/v_{ld} decreases as Wo increases and peaks disappear when Wo = 4.5–6.3.

It can be seen that higher velocity values are located near the leading wall of the cavity at low Wo number and at $Re_{Dh} \approx 100$. As Re_{Dh} increases, higher velocity values are distributed near the trailing wall of the cavity. However, as Wo number increases (Wo = 4.5–6.3) velocity distribution across the center of primary vortex becomes nearly constant regardless of Re_{Dh}.

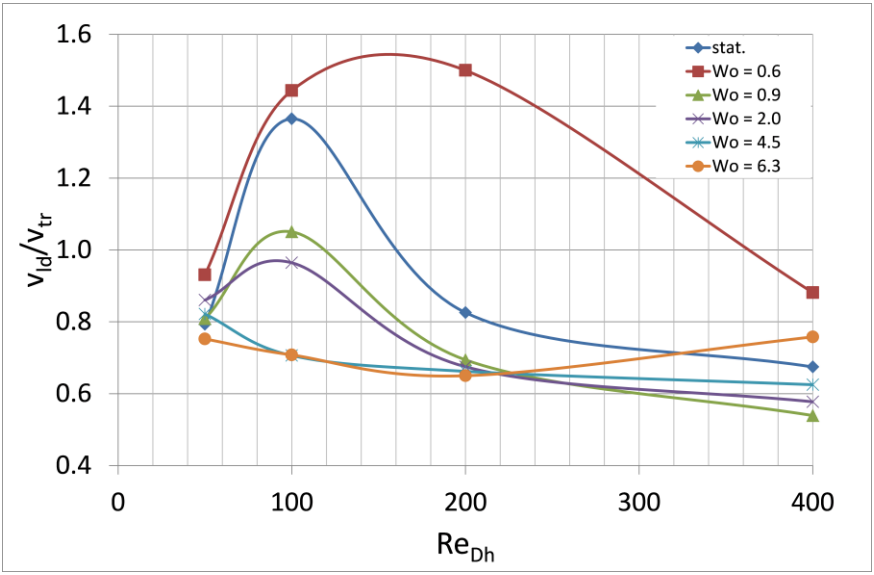

Fig. 28. The ratio of velocities near the leading wall (v_{ld}) to maximum velocity near the trailing wall (v_{tr}) of cavity across the center of the primary vortex

CONCLUSIONS

In the thesis flow structure and dynamics in cavities were investigated combining experimental flow visualization and CFD methods.

1. In transitional and closed-type cavities ($L/h_1 \geq 8$) and in the case of laminar flow regime, separated shear layer reattaches to the bottom wall of the cavity and stable recirculation zone is formed which length x_r/h_1 depends on Re_{h1} and H/h and can be expressed as $(x_r/h_1)\left(\frac{H}{h}\right) = 0.35Re_{h1}^{0.7}$. This relation is valid until the transitional flow regime is reached.

2. In the transitional type cavity ($8 \leq L/h \leq 12$) and in the case of laminar flow regime forward-facing step influences flow structure when recirculation zone reaches middle-part of the cavity ($x_r/h_1 \approx (0.5–0.6)L$). In that case, the reattaching shear layer is lifted from the bottom wall of the cavity and a stagnant recirculation loop is formed. This structure breaks after the transition to a turbulent flow regime. In the initial and final stages of the transitional flow regime, a two-vortex flow structure with a saddle point between them is formed.

3. In transitional and closed-type cavities ($L/h_1 \geq 8$) turbulent flow regime ($Re_{h1} > 400$) is characterized by the formation of instantaneous vortices and instabilities in recirculating flow. It determines the increased interaction of the separated shear layer and recirculating flow in the cavity, which leads to faster shear layer reattachment. In turbulent flow regime relative recirculation zone length approaches asymptotical value in the range of $x_r/h_1 = 6–8$ and can be estimated as $\left(\frac{x_r}{h_1}\right) = 7 + 50\mathrm{Re}_{h1}^{-0.55}$. In this case, recirculation zone length is less depended on cavity geometrical parameters because the system of at least three periodically formed and detached vortices are formed behind the backward-facing step. It is conditioned by the growing main (primary) vortex in the recirculation zone until its size reaches the critical value, restricted by the cavity lid. Consequently, this vortex is detached from the backward-facing step of the cavity and a system of new vortices begins to develop.

4. Channel expansion ratio (H/h) determines the adverse pressure gradient in the cavity and its stabilizing effect for recirculation zone length. This effect can be related to the law of free stream spreading and expressed as $(v_1-v_2)/(v_1+v_2) = f(H/h)$. The value of $H/h \approx 2.5 \pm 0.5$ depicts a point of fundamental change above which relative recirculation zone length x_r/h_1 depending on Re gradually increases approaching asymptotical value as H/h increases.

5. In the open-type cavity ($L/h_1 < 6$) separated shear layer does not reattach to the bottom wall of the cavity. The flow structure depends on the depth of the cavity which determines the number of vortices in the cavity In the present case ($L/h_1 = 0.5$), two vortices systems are formed in the cavity.

5.1. Flow in the open-type cavity is two-dimensional in the case of the laminar flow regime and changes to three-dimensional when $Re_{Dh} \geq 1000$.

Three-dimensional flow is characterized by vortices bifurcation and transversal flows across the center of the primary vortex.

5.2. Velocity distribution across the center of primary vortex depends on Re_{Dh} and Wo_{Dh} numbers. When Wo_{Dh} is low ($Wo_{Dh} \leq 2$) maximum velocity changes its location between leading and trailing walls of the cavity depending on Re_{Dh}. In the case of high Wo_{Dh} (Wo_{Dh} = 4.5–6.3) maximum velocity is located near the trailing wall of the cavity in the whole investigated Re_{Dh} range (Re_{Dh} = 50–400).

REFERENCES

1. ANASTASIOU, A. D., SPYROGIANNI, A. S., PARAS, S. V. Experimental study of pulsatile blood flow in micro channels. *19th International Congress of Chemical and Process Engineering*. 2010, Prague, Chech Republic.

2. ARMALY, B. F., DURST F., PEREIRA J. C. F., SCHÖNUNG B. Experimental and theoretical investigation of backward-facing step flow. *Journal of Fluid Mechanics*. 1983, 127(1), 473. ISSN 0022-1120.

3. BACK, L. H., ROSCHKE, E. J. Shear-Layer Flow Regimes and Wave Instabilities and Reattachment Lengths Downstream of an Abrupt Circular Channel Expansion. *Journal of Applied Mechanics*. 1972, 39(3), 677–681. ISSN 0021-8936.

4. BASU, M., ZAHOOR, A., KHAN, R. A. Review of fluid flow and heat transfer through microchannels. *International Journal of Scientific and Technical Advancements*. 2019, 5(1), 17–20.

5. CANTWELL, C. D., BARKLEY, D., BLACKBURN, H. M. Transient growth analysis of flow through a sudden expansion in a circular pipe. *Physics of Fluids*. 2010, 22(3), 034101. ISSN 1070-6631.

6. CARLSOHN, M. F., KEMMLING, A., PETERSEN, A., WIETZKE L. 3D real-time visualization of blood flow in cerebral aneurysms by light field particle image velocimetry. Proc. SPIE 9897, Real-Time Image and Video Processing 2016.

7. CARVALHO, M. G., DURST, F., PEREIRA, J. C. F. Predictions and measurements of laminar flow over two-dimensional obstacles. *Applied Mathematical Modelling*. 1987, 11(1), 23–34. ISSN 0307904X.

8. CHEN, L., ASAI, K., NONOMURA, T., XI, G., LIU, T. A review of Backward-Facing Step (BFS) flow mechanisms, heat transfer and control. *Thermal Science and Engineering Progress*. 2018a, 6, 194–216. ISSN 24519049.

9. CHEN, X., LI, T., ZENG, H., HU, Z., FU, B. Numerical and experimental investigation on micromixers with serpentine microchannels. *International Journal of Heat and Mass Transfer*. 2016, 98, 131–140. ISSN 00179310.

10. COLEMAN, S. E., NIKORA, V. I., MCLEAN, S. R., SCHLICKE, E. Spatially Averaged Turbulent Flow over Square Ribs. *Journal of Engineering Mechanics*. 2007, 133(2), 194–204. ISSN 0733-9399.

11. COUTANCEAU, M., MIGEON, C., EHRMANN, P. Particulars of the cross- and spanwise near-wake development of a short Semicircular-section Shell, through the TransitionRe-range ($60 \leq Re \leq 600$). *Journal of Visualization*. 2000, 3(1), 9–26. ISSN 1343-8875.

12. D'ADAMO, J., SOSA, R., ARTANA, G. Active Control of a Backward Facing Step Flow With Plasma Actuators. *Journal of Fluids Engineering*. 2014, 136(12), 121105. ISSN 0098-2202.

13. DEJOAN, A., JANG, Y.-J., LESCHZINER, M. A. Comparative LES and Unsteady RANS Computations for a Periodically-Perturbed Separated Flow Over a Backward-Facing Step. *Journal of Fluids Engineering*. 2005, 127(5), 872–878. ISSN 0098-2202.

14. ESTEVE, M. J., REULET, P., MILLAN, P. Flow field characterization within a rectangular cavity. *10th International Symposium Applications of Laser Techniques to Fluid Mechanics*. 2000, Lisbon, Portugal.

15. FAURE, T. M., PASTUR, L., LUSSEYRAN, F., FRAIGNEAU Y., BISCH, D. Three-dimensional centrifugal instabilities development inside a parallelepipedic open cavity of various shape. *Experiments in Fluids*. 2009, 47(3), 395–410. ISSN 0723-4864.

16. FELDMAN, Y. Theoretical analysis of three-dimensional bifurcated flow inside a diagonally lid-driven cavity. *Theoretical and Computational Fluid Dynamics*. 2015, 29(4), 245–261. ISSN 0935-4964.

17. FERNANDO, J. N., KRIEGSEIS, J., RIVAL, D. E. On the separated region behind a confined backward-facing step. *20th Annual Conference of the CFD Society of Canada (CFDSC)*. 2012, Canmore, Canada.

18. GOHARZADEH, A., RODGERS, P. Experimental Measurement of Laminar Axisymmetric Flow Through Confined Annular Geometries With Sudden Inward Expansion. *Journal of Fluids Engineering*. 2009, 131(12), 124501. ISSN 0098-2202.

19. GONG, S. C., LIU, R. G., CHOU, F. C., CHIANG, A. S. T. Experiment and simulation of the recirculation flow in a CVD reactor for monolithic materials. *Experimental Thermal and Fluid Science*. 1996, 12(1), 45–51. ISSN 08941777.

20. GUAN, G., WU, L., BHADAT, A. A. S., LI, Z., CHEN, P. C. Y., CHAO, S., ONG, C. J., HAN, J. Spiral microchannel with rectangular and trapezoidal cross-sections for size based particle separation. *Scientific Reports*. 2013, 3, 1475. ISSN 20452322.

21. GURCAN, F. Streamline Topologies in Stokes Flow Within Lid-Driven Cavities. *Theoretical and Computational Fluid Dynamics*. 2003, 17(1), 19–30. ISSN 0935-4964.

22. HADDADI, H., DI CARLO, D. Inertial flow of a dilute suspension over cavities in a microchannel. *Journal of Fluid Mechanics*. 2017, 811, 436–467. ISSN 0022-1120.

23. HENDERSON, J., BADCOCK, K., RICHARDS, B. E. Subsonic and transonic transitional cavity flows. *6th Aeroacoustics Conference and Exhibit*. 2000, Reston, Virigina: American Institute of Aeronautics and Astronautics.

24. JANG, Y.-H., KWON, C. H., KIM, S. B., SELIMOVIC, Š., SIM, W.-Y., BAE, H., KHADEMHOSSEINI, A. Deep wells integrated with microfluidic valves for stable docking and storage of cells. *Biotechnology Journal*. 2011, 6(2), 156–164. ISSN 18606768.

25. JAYARAJ, S., SALEEL, C. A., SHAIJA, A. On simulation of backward facing step flow usig immersed boundary method. *International Journal of Advanced Computer Science*. 2013, 3(4), 164–174.

26. JUNG, J., KUO, C.-J., PELES, Y., AMITAY, M. The flow field around a micropillar confined in a microchannel. *International Journal of Heat and Fluid Flow*. 2012, 36, 118–132. ISSN 0142727X.

27. KARIMI, A., YAZDI, S., ARDEKANI, A. M. Hydrodynamic mechanisms of cell and particle trapping in microfluidics. *Biomicrofluidics*. 2013, 7(2), 021501. ISSN 1932-1058.

28. KHABIRY, M., CHUNG, B. G., HANCOCK, M. J., SOUNDARARAJAN, H. C., DU, Y., CROPEK, D., LEE, W. G., KHADEMHOSSEINI, A. Cell Docking in Double Grooves in a Microfluidic Channel. *Small*. 2009, 5(10), 1186–1194. ISSN 16136810.

29. KHERBEET, A. S., MOHAMMED, H. A., MUNISAMY, K. M., SALMAN, B. H. The effect of step height of microscale backward-facing step on mixed convection nanofluid flow and heat transfer characteristics. *International Journal of Heat and Mass Transfer*. 2014, 68, 554–566. ISSN 00179310.

30. KIM, J., ANTAKI, J. F., MASSOUDI, M. Computational study of blood flow in microchannels. *Journal of Computational and Applied Mathematics*. 2016, 292, 174–187. ISSN 03770427.

31. LEONARDI, S., ORLANDI, P., SMALLEY, R. J., DJENIDI, L., ANTONIA, R. A. Direct numerical simulations of turbulent channel flow with transverse square bars on one wall. *Journal of Fluid Mechanics*. 2003, 491, 229–238. ISSN 00221120.

32. LIEBER, B. B., LIVESCU V., HOPKINS, L. N., WAKHLOO, A. K. Particle Image Velocimetry Assessment of Stent Design Influence on Intra-Aneurysmal Flow. *Annals of Biomedical Engineering*. 2002, 30(6), 768–777. ISSN 0090-6964.

33. LIMA, R., WADA, S., TAKEDA, M., TSUBOTA, K., YAMAGUCHI, T. In vitro confocal micro-PIV measurements of blood flow in a square microchannel: The effect of the haematocrit on instantaneous velocity profiles. *Journal of Biomechanics*. 2007, 40(12), 2752–2757. ISSN 00219290.

34. LIMA, R., WADA, S., TANAKA, S., TAKEDA, M., ISHIKAWA, T., TSUBOTA, K.-I., IMAI, Y., YAMAGUCHI, T. In vitro blood flow in a rectangular PDMS microchannel: experimental observations using a confocal micro-PIV system. *Biomedical Microdevices*. 2008, 10(2), 153–167. ISSN 1387-2176.

35. MIGEON, C., PINEAU, G., TEXIER, A. Three-dimensionality development inside standard parallelepipedic lid-driven cavities at Re=1000. *Journal of Fluids and Structures*. 2003, 17(5), 717–738. ISSN 08899746.

36. NILSSON, J., HAMMARSTROM, B., LAURELL, T. Review of cell

and particle trapping in microfluidic systems. *Analytica Chimica Acta*. 2009, 649(2), 141–157. ISSN 00032670.

37. OMORI, T., IMAI, Y., ISHIKAWA, T., YAMAGUCHI, T. Hemodynamics in the Microcirculation and in Microfluidics. *Annals of Biomedical Engineering*. 2015, 43(1), 238–257. ISSN 0090-6964.

38. PEDIŠIUS, A., ŠLANČIAUSKAS, A. Heat Transfer Augmentation in Turbulent Flow. Beggel House, New York, 1995.

39. POURYOUSSEFI, S. G., MIRZAEI, M., HAJIPOUR, M. Experimental study of separation bubble control behind a backward-facing step using plasma actuators. *Acta Mechanica*. 2015, 226(4), 1153–1165. ISSN 0001-5970.

40. RAI, S. K., SHARMA, R., SAIFI, M., TYAGI, R., SINGH, D., GUPTA, H. Review of recent applications of micro channel in MEMS devices. *International Journal of Applied Engineering Research*. 2018, 13(9), 64-69. ISSN 0973-4562.

41. SPAZZINI, P. G., LUSO, G., ONORATO, M., ZURLO, N., CICCA, D., G. M. Unsteady behavior of back-facing step flow. *Experiments in Fluids*. 2001, 30(5), 551–561. ISSN 0723-4864.

42. SU, Y., CHEN, G., KENIG, E. Y. An experimental study on the numbering-up of microchannels for liquid mixing. *Lab on a Chip*. 2015, 15(1), 179–187. ISSN 1473-0197.

43. TIHON, J., PENKAVOVA, V., HAVLICA, J., ŠIMČIK, M. The transitional backward-facing step flow in a water channel with variable expansion geometry. *Experimental Thermal and Fluid Science*. 2012, 40, 112–125. ISSN 08941777.

44. TOJA-SILVA, F., PERALTA, C., LOPEZ-GARCIA, O., NAVARRO, J., CRUZ, I. Effect of roof-mounted solar panels on the wind energy exploitation on high-rise buildings. *Journal of Wind Engineering and Industrial Aerodynamics*. 2015, 145, 123–138. ISSN 01676105.

45. WARD, K., FAN, Z. H. Mixing in microfluidic devices and enhancement methods. *Journal of Micromechanics and Microengineering*. 2015, 25(9), 094001. ISSN 0960-1317.

46. WEE, D., YI, T., ANNASWAMY, A., GHONIEM, A. F. Self-sustained oscillations and vortex shedding in backward-facing step flows: Simulation and linear instability analysis. *Physics of Fluids*. 2004, 16(9), 3361–3373. ISSN 1070-6631.

47. XIA, G., CHEN, Z., CHENG, L., MA, D., ZHAI, Y., YANG, Y. Micro-PIV visualization and numerical simulation of flow and heat transfer in three micro pin-fin heat sinks. *International Journal of Thermal Sciences*. 2017, 119, 9–23. ISSN 12900729.

48. YAO, H., COOPER, R. K., RAGHUNATHAN, S. Numerical Simulation of Incompressible Laminar Flow over Three-Dimensional

Rectangular Cavities. *Journal of Fluids Engineering*. 2005, 126(6), 919–927. ISSN 0098-2202.

49. ZHAI, Y., XIA, G., LI, Z. Micro-PIV study of flow and the formation of vortex in micro heat sinks with cavities and ribs. *International Journal of Heat and Mass Transfer*. 2016, 98, 380–389. ISSN 00179310.

50. ZHOU, J., KASPER, S., PAPAUTSKY, I. Enhanced size-dependent trapping of particles using microvortices. *Microfluidics and Nanofluidics*. 2013, 15(5), 611–623. ISSN 1613-4982.

PUBLICATIONS RELATED TO THE DISSERTATION

Publication in the journal of "Clarivate Analytics – Web of Science Core Collection"

1. VENSLAUSKAS M., OSTAŠEVIČIUS V., VILKINIS P. Influence of low-frequency vibrations on blood flow improvement in human‘s limbs. Bio-medical materials and engineering. 2017, 28(2), 117-130. ISSN 0959-2989.
2. VILKINIS P., PEDIŠIUS N., VALANTINAVIČIUS M. Investigation of flow dynamics over transitional-type microcavity. Journal of fluids engineering. 2018, 140(7), 071203-1-071203-7. ISSN 0098-2202

Articles in other scienrtific journals

1. VILKINIS P., PEDIŠIUS N., VALANTINAVIČIUS M. Vandens tekėjimo mikrokanale tyrimas dalelių vizualizacijos metodu. Energetika. 2015, 61(2), 189-205. ISSN 0235-7208.
2. VILKINIS P., VALANTINAVIČIUS M., PEDIŠIUS N. Investigation of fluid structure in open type cavity under stationary and pulsatile flow conditions. Energetika. 2016, 62(1-2), 37-44. ISSN 0235-7208.

Publication in the international conferences

1. VILKINIS P., PEDIŠIUS N., VALANTINAVIČIUS M. Investigation of pulsating flow in open type microcavity. *14th Annual international conference of young scientists on energy issues* (CYSENI 2017), Kaunas, Lithuania, May 25-26, 2017. Kaunas: LEI, 2017. p. 308-315. ISSN 1822-7554
2. VILKINIS P., PEDIŠIUS N. Parametric analysis of recirculating flow dynamics in microcavity. *15th Annual international conference of young scientists on energy issues* (CYSENI 2018), Kaunas, Lithuania, May 23-25, 2018. Kaunas: LEI, 2018. p. 353-359. ISSN 1822-7554
3. VILKINIS P., PEDIŠIUS N. Investigation of primary vortex structure in open type cavity. *16th Annual international conference of young scientists on energy issues* (CYSENI 2019), Kaunas, Lithuania, May 23-24, 2019. Kaunas: LEI, 2019. p. 330-340. ISSN 1822-7554

Presentations at international conferences

1. VILKINIS P., PEDIŠIUS N., VALANTINAVIČIUS M. Investigation of fluid flow structure in open type cavity under stationary and pulsatile flow conditions. *13th Annual international conference of young scientists on energy issues* (CYSENI 2016), Kaunas, Lithuania, May 26-27. 2016. Kaunas: LEI, 2016. p. 200. ISSN 1822-7554
2. VILKINIS P., PEDIŠIUS N., VALANTINAVIČIUS M. Investigation of pulsating flow in open type microcavity. *14th Annual international conference of young scientists on energy issues* (CYSENI 2017), Kaunas, Lithuania, May 25-26, 2017. Kaunas: LEI, 2017. p. 308-315. ISSN 1822-7554
3. VILKINIS P., PEDIŠIUS N. Parametric analysis of recirculating flow dynamics in microcavity. *15th Annual international conference of young scientists on energy issues* (CYSENI 2018), Kaunas, Lithuania, May 23-25, 2018. Kaunas: LEI, 2018. p. 353-359. ISSN 1822-7554
4. VILKINIS P., PEDIŠIUS N. Investigation of flow dynamics over microcavities with different inlet types. *The 12th European Fluid Mechanics Conference (EFMC12),* Vienna, Austria, September 9-13, 2018.
5. VILKINIS P., PEDIŠIUS N. Investigation of primary vortex structure in open type cavity. *16th Annual international conference of young scientists on energy issues* (CYSENI 2019), Kaunas, Lithuania, May 23-24, 2019. Kaunas: LEI, 2019. p. 330-340. ISSN 1822-7554
6. VILKINIS P., PEDIŠIUS N. The analysis of recirculation zone dynamics in cavity flow. *17th European Turbulence Conference (ETC17)*, Turin, Italy, September 3-6, 2019

Brief information about the author

Personal data:

Name: Paulius

Surname: Vilkinis

Date of birth: July 10, 1989

Place of birth: Vilnius, Lithuania

e-mail: paulius.vilkinis@lei.lt

Education:

2008 – 2012 Bachelor's degree in Energetic Physics at Vytautas Magnus University

2012 – 2014 Master's degree in Physics at Vytautas Magnus University

2015 – 2019 Doctoral studies in Energetic and Power Engineering at Lithuanian Energy Institute

REZIUMĖ

Skysčio srauto dinamikos ir struktūros tyrimas kanaluose su struktūrizuotais paviršiais

Tarp srautų dinamikos tyrimų svarbią vietą užima srauto atitrūkimo reiškinių, kurie sutinkami daugelyje tekėjimų ir vis dar kelia nemažai praktinių ir mokslinių problemų, tyrimai. Srauto atitrūkimas, sukeliamas teigiamo slėgio gradiento, kurį, savo ruožtu, lemia staigūs kanalo skerspjūvio pokyčiai. Srauto atitrūkimas turi didžiulę įtaką masės, impulso ir šilumos mainų pernašos bei srauto maišymosi procesams. Šie procesai ir jų svarba įvairiuose inžineriniuose uždaviniuose lemia didėjantį susidomėjimą fundamentiniais srauto atitrūkimo reiškinių tyrimais (Chen, Asai, Nonomura, Xi, & Liu, 2018). Šie tyrimai taip pat leidžia giliau suprasti vidinį sūkurių formavimosi, tarpusavio sąveikos ir jų subyrėjimo mechanizmus. Be viso to, šios žinios suteikia galimybę kurti naujus ir tobulinti bei tikslinti jau esamus skaitinio modeliavimo metodus.

Naujų eksperimentinių tyrimo metodų taikymas išplečia galimybes giliau pažvelgti į tekėjimo struktūrą. Dėl spartaus srautų vizualizacijos metodų tobulėjimo per pastaruosius 20 metų tapo galima sudėtingų tekėjimo struktūrų analizė, atskleidžiant sūkurių formas, jų parametrus ir formavimosi eigą. Tai rodo ir didėjantis mikrosrautų vizualizacijos (μPIV) naudojimas srauto struktūros tyrimuose (Basu, Zahoor, & Khan, 2019; Xia et al., 2017; Zhai, Xia, Chen, & Li, 2016). Srautų vizualizacijos sistema leidžia atlikti tikslius, netrikdančius srauto, tekėjimo parametrų matavimus. Šio eksperimentinio metodo derinimas kartu su skaitiniais tekėjimo analizės metodais papildo vienas kitą tiek kokybiniais, tiek kiekybiniais duomenimis. Mikrosrautų vizualizacijos sistemos taikymas supaprastina tyrimus suteikdamas galimybę stambiu planu stebėti sraute vykstančius procesus.

Apskritai, procesai, vykstantys nedidelio skersmens kanaluose, kelia vis didesnį susidomėjimą dėl didėjančio pritaikymo įvairiose srityse praktikoje. Struktūrizuoti, nedidelio skersmens kanalai dėl didelio paviršiaus ploto ir tūrio santykio susilaukia dėmesio projektuojant aušinimo įrenginius elektronikoje (Basu et al., 2019; Rai et al., 2018; Xia et al., 2017). *Lab-on-chip* ir mikroelektromechaninių sistemų tobulėjimas ir platėjantis taikymas lemia maišymosi procesų analizės plėtrą mažo skersmens kanaluose (X. Chen, Li, Zeng, Hu, & Fu, 2016; Su, Chen, & Kenig, 2015; Ward & Fan, 2015). Dėl nedidelio naudojamo fluido tūrio nedidelio skersmens kanaluose jie tapo labai paklausūs biomedicinos inžinerijoje. Dėl šlyties sluoksnio ir recirkuliacinio tekėjimo susiformavimo struktūrizuotos formos kanalai naudojami ląstelių nusodinimo (Jang et al., 2011; Khabiry et al., 2009) uždaviniuose. Kavernose susiformavę sūkuriai yra efektyvūs dalelių gaudymo (Karimi, Yazdi, & Ardekani, 2013; Nilsson, Evander, Hammarström, & Laurell, 2009; Zhou,

Kasper, & Papautsky, 2013) ir atskyrimo (Guan et al., 2013) uždaviniuose. Nedidelis kanalo skersmuo ir įvairios formos kavernos yra patogios naudoti kraujo tekėjimo (Anastasiou, Spyrogianni, & Paras, 2010; Kim, Antaki, & Massoudi, 2016; Lima, Wada, Takeda, Tsubota, & Yamaguchi, 2007; Lima et al., 2008; Omori, Imai, Kikuchi, Ishikawa, & Yamaguchi, 2015) bei krešulių susidarymo ir aneurizmų tyrimams (Carlsohn, Kemmling, Petersen, & Wietzke, 2016; Lieber, Livescu, Hopkins, & Wakhloo, 2002) kraujotakos sistemoje.

Tyrimo objektas

Hidrodinaminiai masės pernašos procesai kavernose.

Darbo tikslas

Darbo tikslas – eksperimentiniais ir skaitiniais metodais ištirti skysčio srauto dinamiką ir struktūrą kanaluose su staigiais jo skerspjūvio pokyčiais ir nustatyti recirkuliacinių tekėjimų savybių priklausomumus nuo tekėjimo režimų ir geometrinių parametrų.

Darbo uždaviniai

Darbo tikslui pasiekti iškelti šie uždaviniai:

1. Nustatyti recirkuliacinės zonos ilgio kitimo dėsningumus pereinamojo ir uždarojo tipo kavernose esant laminariniam tekėjimo režimui.
2. Nustatyti recirkuliacinės zonos ilgio kitimo ir struktūros ypatumus pereinamojo tipo kavernoje priklausomai nuo tekėjimo režimo.
3. Nustatyti recirkuliacinės zonos ilgio kitimo dėsningumus pereinamojo ir uždarojo tipo kavernose esant turbulentiniam tekėjimo režimui.
4. Ištirti kanalo išplatėjimo santykio įtaką recirkuliacinės zonos ilgio dinamikai pereinamojo ir uždarojo tipo kavernose.
5. Ištirti recirkuliacinės zonos tekėjimo struktūrą gilioje atvirojo tipo kavernoje priklausomai nuo tekėjimo režimo.

Ginamieji teiginiai

1. Laminariniame tekėjimo režime pereinamojo ir uždarojo tipo kavernose recirkuliacinės zonos struktūra yra stabili ir jos ilgis x_r/h_1 yra funkcija, priklausanti nuo Re_{h1} ir H/h.
2. Turbulentiniame tekėjimo režime pereinamojo ir uždarojo tipo kavernose, recirkuliacinėje zonoje, formuojasi periodiškai atitrūkstančių ir iš naujo susidarančių sūkurių sistema, todėl santykinis recirkuliacinės zonos ilgis, didėjant Re_{h1}, nebepriklauso nuo kavernos geometrinių parametrų.
3. Kanalo išplatėjimo santykiui H/h pasiekus kritines vertes, recirkuliacinės zonos ilgis, didėjant Re_{h1}, laipsniškai didėja, artėdamas

prie pastovios asimptotinės reikšmės, būdingos turbulentiniam tekėjimo režimui.

4. Gilioje atvirojo tipo kavernoje formuojasi sudėtinga trimatė tekėjimo struktūra, pasižyminti skersiniais pertekėjimais, sukeliančiais sūkurių pasidalinimą turbulentiniame tekėjimo režime.
5. Didelio dažnio pulsuojantis tekėjimas stabilizuoja greičio pasiskirstymą gilioje atvirojo tipo kavernoje.

Mokslinis naujumas

Šiuo darbu papildytos žinios apie recirkuliacinės zonos struktūrą ir ilgio dinamiką skirtingo tipo kavernose priklausomai nuo kavernos geometrinių parametrų (H/h, L/h1). Esant stabiliems laminariniam ir turbulentiniam tekėjimo režimams nustatyti priklausomumai ir fizikinių parametrų kitimo dėsningumai, susiejant juos su laisvų srovių plitimo dėsningumais. Disertacijoje atskleistos H/h ir Re poveikio recirkuliacinio tekėjimo zonos dinamikai priežastys leidžia paaiškinti įvairių autorių rezultatų sklaidą ir apibendrinti juos universaliomis išraiškomis, būdingomis laminariniam ir turbulentiniam tekėjimo režimams.

Parodyta, kad gilioje atvirojo tipo kavernoje turbulentinio tekėjimo režimo metu įvyksta sūkurio pasidalinimas į dvi simetriškas trimates struktūras, nulemtas vidinių pertekėjimų.

Praktinė vertė

Taikomąją reikšmę lemia didelis kiekis praktinių uždavinių, kuriuose atitrūkstamus tekėjimus sukelia staigūs kanalo skerspjūvio pokyčiai, kurie gali būti analizuojami kaip įvairaus tipo kavernų kanalo sienelėse aptekėjimai. Šios žinios naudingos projektuojant srauto matuoklius, šilumos mainų ir maišymosi įrenginius, taip pat tobulinant CFD modelius.

Nustatyti priklausomumai leidžia įvertinti atitrūkusio šlyties sluoksnio prisijungimo prie kavernos dugno padėtį atsižvelgiant į tekėjimo režimą ir kavernos geometrinius parametrus. Prisijungimo zona pasižymi suaktyvėjusiais šilumos mainais ir slėgio pokyčiais toje zonoje. Dėl šių priežasčių fundamentinės žinios apie tekėjimo dinamiką kavernoje yra naudingos daugelyje praktinių uždavinių.

Autoriaus indėlis

Disertacijos autorius išanalizavo mokslinius duomenis apie fluido tekėjimo dėsningumus įvairios formos kanaluose su kliūtimis ir kavernose bei eksperimentinį ir skaitinį šių dėsningumų tyrimo būdus. Autorius atliko eksperimentinius, pasinaudodamas sistema µPIV, ir skaitinius, pasinaudodamas programine įranga ANSYS *Fluent*, recirkuliacinės zonos ilgio ir srauto struktūros topologijos tyrimus atvirojo, pereinamojo ir uždarojo tipo kavernose

plačiame Re skaičiaus intervale bei keičiantis kavernos geometriniams parametrams. Autorius nustatė recirkuliacinės zonos ilgio dinamikos dėsningumus skirtingo tipo kavernose ir pateikė priklausomybes, leidžiančias įvertinti santykinį recirkuliacinės zonos ilgį laminariniame ir turbulentiniame tekėjimo režimuose. Taip pat nustatė sūkurių topologijos kitimo dėsningumus priklausomai nuo tekėjimo režimo gilioje atvirojo tipo kavernoje.

Mokslinė sklaida

Disertacijoje pateikti tyrimų rezultatai paskelbti dvejuose moksliniuose straipsniuose, esančiuose „Clarivate Analytics“ duomenų bazėje „Web of Science Core Collection“ referuojamuose žurnaluose, turinčiuose citavimo indeksą, ir dvejuose moksliniuose straipsniuose, registruotuose tarptautinėse mokslinės informacijos duomenų bazėse. Taip pat tyrimų rezultatai pristatyti šešiose tarptautinėse konferencijose.

IŠVADOS

Derinant dalelių judėjimo sraute vizualizaciją ir skaitinį vidutinių ir momentinių greičio laukų modeliavimą, ištirta tekėjimo kavernose dinamika ir struktūra, keičiant kavernos ilgį, gylį ir tekėjimo režimą. Gauti rezultatai leidžia daryti tokias išvadas:

1. Pereinamojo ir uždarojo tipo kavernose ($L/h_1 > 8$), esant laminariniam tekėjimo režimui, atitrūkęs šlyties sluoksnis prisijungia prie kavernos dugno ir už jos atgalinės sienelės formuojasi stabilus recirkuliacinis kontūras, kurio santykinį ilgį x_r/h_1 lemia Re_{h1} ir H/h. Šis dėsningumas iki pereinamojo tekėjimo režimo pradžios aprašomas priklausomybe: $(x_r/h_1)\left(\frac{H}{h}\right) = 0{,}3Re_{h1}^{0,75}$.
2. Pereinamojo tipo kavernoje ($8 \leq L/h_1 \leq 12$), esant laminariniam tekėjimo režimui ir recirkuliacinei zonai pasiekus kavernos vidurį ($x_r/h_1 \approx$ (0,5–0,6)L), priekinė sienelė pradeda daryti įtaką tekėjimo struktūrai. Dėl jos poveikio prisijungiantis šlyties sluoksnis atkeliamas nuo kavernos dugno ir visoje kavernoje susidaro stovintis recirkuliacinis kontūras, kurį suardo tik tekėjimo kanale perėjimas į turbulentinį tekėjimo režimą. Šio recirkuliacinio tekėjimo pradinėje ir galutinėje stadijoje susidaro dviejų sūkurių sistema su balno tipo skiriamąja zona, kurioje šlyties įtempiai ant kavernos dugno yra minimalūs.
3. Pereinamojo ir uždarojo tipo kavernose ($L/h_1 \geq 8$), kai $Re_{h1} > 400$, įvyksta perėjimas į turbulentinį tekėjimo režimą, kuriam būdingas nestabilumų susidarymas kavernoje. Tai stiprina atitrūkusio šlyties sluoksnio sąveiką su recirkuliaciniu tekėjimu ir greitina jo prisijungimą prie kavernos dugno. Turbulentiniame tekėjimo režime artėjama link asimptotinio dėsningumo $\left(\frac{x_r}{h_1}\right) = 7 + 50Re_{h1}^{0,55}$, kai recirkuliacinės zonos ilgis artėja vertę, lygią x_r/h_1 = 6–8. Tai lemia sūkurių sistemos už laipto formavimasis, kurią sudaro mažiausiai trys periodiškai atsinaujinantys sūkuriai. Šlities sluoksniui atitrūkus nuo atgalinės kavernos briaunos, formuojasi pirminis sūkurys, kuris didėdamas generuoja recirkuliacinėje zonoje kitus sūkurius. Pirminiam sūkuriui pasiekus kritinį dydį, lygų kavernos gyliui, jis atitrūksta. Šis procesas periodiškai atsikartoja ir paaiškina recirkuliacinės zonos ilgio priklausomumą nuo kavernos gylio.
4. Parametras H/h (kanalo išplatėjimo santykis) parodo stabilizuojantį teigiamo slėgio gradiento poveikį recirkuliacinei zonai kavernoje. Šio poveikio dėsningumas siejasi su laisvos srovės plitimo nejudančioje aplinkoje arba pasroviui tekančiame sraute pobūdžiu ir gali būti išreikštas priklausomumu $(v_1\text{-}v_2)/(v_1+v_2) = f(H/h)$. $H/h \approx 2{,}5 \pm 0{,}5$ reikšmė parodo priklausomumo esminio pokyčio vietą, nuo kurios santykinis

recirkuliacinės zonos ilgis x_r/h_1, didėjant H/h ir Re, tolygiai didėja artėdamas prie asimptotinės reikšmės.

5. Atvirojo tipo kavernoje ($L/h_1 < 6$) šlyties sluoksnio prisijungimas prie kavernos dugno nevyksta, bet tekėjimo struktūra kavernoje priklauso nuo jos gylio, kuris lemia pagrindinių sūkurių kiekį sistemoje. Kai $L/h_1 = 0,5$, kavernoje formuojasi dviejų pagrindinių sūkurių sistema.

5.1 Tekėjimas gilioje atvirojo tipo kavernoje yra dvimatis esant laminariniam tekėjimo režimui kanale ir pasikeičia į trimatį, kai $Re_{Dh} \geq 1000$. Trimatiškumas pasireiškia sūkurių pasidalinimu kavernoje ir skersiniais pertekėjimais per plokštumą, kertančią pirminio sūkurio centrą.

5.2 Esant pulsuojančiam tekėjimo režimui, greičio pasiskirstymas atvirojo tipo kavernoje priklauso nuo Re ir Wo. Esant mažoms Wo_{Dh} ($Wo_{Dh} \leq 2$) vertėms, maksimalus greitis keičia savo padėti nuo atgalinės link priekinės kavernos sienelės priklausomai nuo Re_{Dh}. Kai Wo_{Dh} vertės didelės ($Wo_{Dh} = 4,5–6,3$) maksimalus greitis išlieka ties priekine kavernos sienele visame tirtame Re_{Dh} verčių intervale ($Re_{Dh} = 50–400$).

PADĖKA

Pirmiausia dėkoju moksliniam vadovui dr. Nerijui Pedišiui už vadovavimą ir pagalbą rengiant disertaciją ir habil. dr. Antanui Pedišiui už vertingus patarimus ir suteiktas mokslines žinias. Taip pat dėkoju visiems laboratorijos ir instituto darbuotojams, kurie tiesiogiai ar netiesiogiai prisidėjo prie mokslinių tyrimų.

Dėkoju disertacijos recenzentams dr. Raimondui Pabarčiui, dr. Algiui Džiugiui ir dr. Egidijui Urbonavičiui už vertingas pastabas ir komentarus.

Taip pat dėkoju studijų administratorei Jolantai Kazakevičienei už pagalbą sprendžiant su doktorantūros studijomis susijusius klausimus.

Pabaigoje norėčiau padėkoti savo tėvams ir žmonai Viktorijai už kantrybę, palaikymą ir supratingumą.

UDK 532.5(043.3)

SL344. 2019-12-03, 4 leidyb.apsk.1. Tiražas 50 egz.
Išleido Kauno technologijos universitetas, K. Donelaičio g. 73, 44249 Kaunas
Spausdino leidyklos „Technologija“ spaustuvė Studentų g. 54, 51424 Kaunas